EFFECT OF DIP ON THE SUBSURFACE STORAGE OR DISPOSAL OF FLUIDS IN SALINE AQUIFERS

A Thesis

Submitted to the Graduate Faculty of the
Louisiana State University and
Agricultural and Mechanical College
in partial fulfillment of the
requirements for the degree of
Master of Science

in

The Department of Petroleum Engineering

by
Joseph Anthony D'Amico
B.S., Louisiana State University, 1970
August, 1975

ACKNOWLEDGMENT

The author is gratefully indebted to Dr. Oscar K. Kimbler, Professor of Petroleum Engineering, under whose guidance and supervision this work was accomplished.

Likewise, special words of gratitude are extended to: Professor Raphael G. Kazmann, Professor of Civil Engineering, for his constructive comments and suggestions during the course of this study; Mr. Tony Owens, whose assistance expedited the completion of this work; and Mary H. Alston, who typed this manuscript. The author extends his sincere appreciation to Dr. Walter Whitehead, Assistant Professor of Petroleum Engineering, for his invaluable assistance in all phases of the project.

Finally, to my wife, Cathie, for her patience, encouragement, and sacrifices, I humbly dedicate this thesis.

This investigation was financed through funds made available by the Office of Water Resources Research (now the Office of Water Research and Technology), U.S. Department of the Interior, under P.L. 88-379, and administered by the Louisiana Water Resources Research Institute as project A-034-LA.

CONTENTS

LIST OF TABLES

LIST OF FIGURES

ABSTRACT

Previous investigators have established the feasibility of utilizing horizontal, saline aquifers for cyclic storage of fresh water. Additional studies, employing a two-dimensional, radial miniaquifer, have shown that the recovery efficiency in a dipping system is lower than in a similar horizontal system.

The purpose of the present study was to determine the effect of dip on the configuration, migration, and recovery of a "bubble" of injected fresh water in a dipping aquifer of infinite areal extent utilizing a three-dimensional, rectangular miniaquifer. Analog fluids were used with the injected fluid being more dense than the in-place (native) fluid.

Applied to the injection of fresh water in a sal- aquifer, experimental results showed that the lower surface of the injected bubble would not migrate and would remain radial. However, the upper surface would slide updip for all cases investigated. The range of dip angles studied varied from five to twenty degrees.

As the dip angle became progressively larger and as the size of the injected bubble increased the velocity of the upper surface increased, although the lower surface of the injected bubble neither moved nor grew. Also, for

aquifers dipping at five degrees or less the velocity of migration of the upper surface of the bubble may be approximated by a constant multiplied by the sine of the dip angle.

A computer program utilizing a two-dimensional model to predict the configuration of an injected bubble was adapted to describe a three-dimensional case. This necessitated inclusion of gravitational inclination of the displacement boundary.

The results of this study are applicable to miscible displacement processes wherever a density difference exists between native and injected fluids in a dipping aquifer. Subsurface disposal of water-soluble wastes and enhanced recovery operations in the petroleum industry are two such examples outside the field of subsurface storage of fresh water.

CHAPTER I

INTRODUCTION

Storing fresh water, so that an adequate supply is continually available, is a problem that has plagued man for centuries. This problem has been further complicated by two factors resulting from today's society: (1) the large increase in the annual use of fresh water associated with the growth of urban areas and the increased concentration of people and industry, and (2) the increase in the likelihood of industrial or municipal pollution of the streams, rivers, and lakes normally used to supply the fresh water. In the event of degradation of a water source, municipalities must have either an alternate source of fresh water readily available or they must have ample storage facilities. Storage requirements of an urban area are large if both industrial and domestic needs are to be supplied for a long period. Where seasonal rainfall is the primary source of fresh water, large storage facilities are mandatory to maintain a sufficient supply the year around even if there is no threat of pollution.

In areas where the topography is suitable, the construction of dams to create reservoirs is one answer to the storage problem. However, the initial costs may be

prohibitive and the inundation of large areas of land which are capable of serving other purposes may be impracticable or, at the very least, an added expense. In regions of flat topography, ring levees may be constructed to store fresh water. This idea suffers from the same defects as the previous one in that a large land area is required and the initial costs are substantial. Both of these solutions are also adversely affected by pollution, evaporation, and/or seepage.

Another way to store water is to construct steel storage tanks. This eliminates the problems of pollution, seepage, and evaporation. However, large areas of land are a necessity and, excluding land costs, it has been estimated by Kimbler et al.[1] that tank storage in a typical urbanized area is approximately ten cents per gallon of storage capacity (1973 figures). One other argument against the various methods of water storage is the susceptibility of all of them to acts of nature, such as hurricanes, tornadoes, and earthquakes, and to the actions of terrorists.

One alternative to the problems related to surface containment is the storage of fresh water in saline aquifers. Kohout[2] has indicated that saline aquifers underlie numerous regions and may be found at depths as shallow as 500 feet. If a saline aquifer underlies an area, the benefits of subsurface storage are readily apparent in that a minimal amount of land surface is required for injection/production

wells and the initial costs are substantially lower for a system of wells as compared to the construction costs related to either a dam or steel tanks.

The possibility of fresh water storage in saline aquifers has been previously investigated by Kimbler et al.,[1] Cederstrom,[3] Moulder and Frazer,[4] Esmail,[5] Green and Cox,[6] Esmail and Kimbler,[7] Kumar and Kimbler,[8] Francis,[9] Painter,[10] Gelhar et al.,[11] Esmail,[12] Whitehead,[13] and Langhetee.[14] The process consists of injecting fresh water into a saline aquifer when the water supply is abundant. The injected water miscibly displaces the native water and is stored in the aquifer until it is required to replace or supplement the primary water source. The stored water is then produced by pumping the same well or well field, used for injection. Production is stopped when the demand is met or when the salinity of the produced stream reaches an unsatisfactory level. The term "breakthrough" is used to describe the condition when the salinity of the produced stream reaches an unsatisfactory level. Breakthrough in this investigation represents the condition when three percent of the produced stream consist of native fluid. The term "recovery efficiency" is defined as the ratio of the volume of usable water recovered to the total volume injected. Kumar and Kimbler,[8] Gelhar et al.,[11] Esmail,[12] and Whitehead[13] have devised mathematical techniques to predict the recovery efficiency in horizontal aquifers.

The only mathematical model to determine the recovery efficiency and to track the configuration and migration of the injected fresh water in what was intended to approximate a two-dimensional, dipping system was developed by Painter.[10] In his study an analytical solution was derived and experimentally verified for the finite one-dimensional case. Based on this solution, a simplified two-dimensional mathematical technique was developed and confirmed by experimental runs made in a large (105 cm radius), thin (1.10 cm thick) miniature aquifer (miniaquifer).

This study extends Painter's[10] work to a three-dimensional system. It investigates the configuration, migration, and recovery of fresh water injected into a dipping saline aquifer. Painter's[10] two-dimensional mathematical technique was adapted to a three-dimensional system and verified by one set of experimental runs made in a large rectangular (146 cm by 305 cm by 3.81 cm thick) miniaquifer. Another group of runs was made in this miniaquifer to determine the recovery efficiency and to provide a standard against which a mathematical model, developed to track the configuration and migration of fresh water injected into a dipping aquifer, could be compared.

Since this study is concerned with miscible displacement operations in a porous medium where a density difference exists between the native and injected fluids, the results are applicable to other miscible displacement

processes. Examples of such processes are the subsurface disposal of water soluble wastes, secondary and tertiary recovery operations in the petroleum industry, and the cycling of retrograde gas-condensate reservoirs.

CHAPTER II

THEORY AND PREVIOUS INVESTIGATIONS

2.1 General

The injection and storage of fresh water in a saline aquifer is a miscible displacement process. The efficiency of this type of process is affected by the following parameters:

(1) molecular diffusion and convective dispersion
(2) gravity segregation
(3) aquifer dip
(4) pre-existing groundwater flow (flux)
(5) viscosity difference between the injected and native fluids
(6) density difference between the native and fresh water

Throughout this study the following assumptions are made:

(1) no pre-existing groundwater movement (flux)
(2) the viscosities of the native and injected fluids are equal.

Therefore, the factors influencing the flow of miscible fluids through a porous medium which are studied in this investigation are: a) mixing of the two fluids due to molecular diffusion and convective dispersion, b) gravitational segregation due to density difference, and c) the effect of aquifer dip.

2.2 Molecular Diffusion and Convective Dispersion

If two miscible fluids of different composition are in contact with an initially sharp interface a transfer of molecules will occur and, as time passes, the sharp interface is replaced by a mixed zone. This process is due to the random motion of molecules and is called molecular diffusion. The mathematical description of this phenomenon is given by Fick's first and second laws in terms of a molecular diffusion coefficient, D. Although this coefficient is a function of concentration, it is usually permissible to use an average value which is treated as independent of concentration.

Additional mixing other than that caused by diffusion will take place when miscible fluids are flowing through a porous medium. This additional mixing is caused by concentration gradients resulting from fluid flow and is called convective dispersion. There are two types of convective dispersion: longitudinal dispersion, which acts in the direction of gross fluid movement and transverse dispersion, which acts perpendicular to flow. Previous investigations by de Josselin de Jong[15] and Pozzi and Blackwell[16] have shown that longitudinal dispersion is 6 to 20 times greater than transverse dispersion.

Raimondi et al.[17] and Hoopes and Harleman[18] have shown that if a fluid moves radially outward from a well (line source) through a porous medium, displacing a fluid

of the same viscosity and density, the mixing of the two fluids can be represented by the differential equation:

$$\frac{\partial C_i}{\partial t} + \frac{Q}{r}\frac{\partial C_i}{\partial r} = \left(\frac{\alpha r}{Q} + D\frac{r^2}{Q^2}\right)\frac{\partial^2 C_i}{\partial t^2} \qquad (2.1)$$

where: C_i = concentration of injected fluid at radius, r, and time, t.

r = radius. (cm)

t = time. (seconds)

$Q = q/(2\pi h\phi)$. (cm^2/sec)

q = volumetric flow rate. (cc/sec)

h = aquifer thickness. (cm)

ϕ = aquifer porosity. (fraction)

D = coefficient of molecular diffusion of fluids in porous medium. (cm^2/sec)

α = longitudinal dispersivity coefficient of porous medium. (cm)

The longitudinal dispersivity coefficient, α, is a characteristic of the porous medium and increases with increasing permeability and with wider particle size distribution.[17] Bentsen and Nielsen[19] and Brigham et al.[20] have shown that α is also a function of the viscosity ratio of the fluids involved. The value of α increases as the viscosity of the displacing fluid decreases relative to that of the displaced.

For the case of continuous fluid injection at a

steady rate with a concentration, C_o at r = 0, Raimondi et al.[17] and Hoopes and Harleman[18] proposed the following solution to equation (2.1):

$$\frac{C_i}{C_o} = \frac{1}{2} \operatorname{erfc}\left[\frac{r^2/2 - Q \cdot t}{(4/3 \cdot \alpha \cdot R^3 \cdot D/Q \cdot R^4)^{1/2}}\right] \qquad (2.2)$$

where: R = radius of injected fluid at time t, assuming no mixing or gravitational segregation. (cm)

erfc (ξ) = complementary error function of ξ.

$$\operatorname{erfc}(\xi) = \frac{2}{\sqrt{\pi}} \int_{\xi}^{\infty} e^{-w^2}\, dw$$

Equation (2.2) satisfies the following boundary conditions:

$$C_i = C_o \quad \text{for} \quad r = 0,\ t > 0$$
$$C_i = 0 \quad \text{for} \quad r = \infty,\ t > 0$$

However, it does not satisfy the initial condition, $C_i = 0$ for r = 0, t = 0; but the equation does hold for distances outside of 10-20 particle diameters from the source. The above solution has been verified experimentally by Bentsen and Nielsen,[19] Hoopes and Harleman,[18] and Esmail and Kimbler.[6] This equation has been generalized by Gardner et al.[21] to include repeated injection and production cycles.

2.3 Gravity Segregation

If two fluids with different densities are in contact in a porous medium, the more dense fluid will sink relative to the less dense due to gravitational forces. This results in a progressive inclination of the boundary between the two fluids. Gravity segregation in a porous medium may be of two types: (1) static and (2) dynamic. Static gravity segregation occurs when there is no bulk flow of fluids except that due to gravity while the dynamic type ensues when gravity segregation takes place during bulk flow. Kumar and Kimbler[8] demonstrated that for a viscosity ratio of one, dynamic and static gravitational segregation are essentially equal and that results obtained from a linear system may be directly applied to the radial system by a simple geometric correction.

Esmail[12] developed the following equation which correlates gravitational segregation in horizontal, isotropic, linear systems:

$$\frac{(\overline{2XL})}{h} = f(\psi) \qquad (2.3)$$

where: $$\psi = \left[\frac{K \cdot g \cdot \Delta\rho \cdot t}{\bar{\mu} \cdot \phi \cdot h}\right]\left[\frac{(\bar{\mu})^{2/3} \cdot S}{(\Delta\rho)^{5/3} \cdot (g)^{1/3}}\right]^{1/2}$$

$\overline{2XL}$ = projection of the interface on the horizontal. (cm)

K = permeability. (cm^2)

g = acceleration due to gravity. (cm/sec^2)

$\Delta\rho$ = density difference between the fluids. (gm/cc)

t = time. (sec)

$\bar{\mu}$ = average viscosity of the two fluids. (poise)

ϕ = porosity. (fraction)

h = aquifer thickness. (cm)

S = density gradient. (gm/cm^4)

All subsequent investigations involving underground storage carried out at Louisiana State University have employed this relationship together with a correction from linear to radial geometry.

2.4 Gross Gravitational Effects in Dipping Systems

If a fluid is injected into a dipping system containing a fluid of a different density, the injected fluid will tend to migrate as a result of gravitational forces. This gross fluid movement results from a component of velocity due to the density difference between the fluids and acts in the direction of dip of the bed. In an earlier study Painter[10] investigated such fluid movement in both linear and radial systems. He presented equations for the updip and downdip frontal positions of the injected fluid in a finite linear system dipping in the x-direction as:

$$X_u = \frac{q_i \cdot t}{2 \cdot A \cdot \phi} + 4.94 \times 10^{-7} \frac{K \cdot \Delta\rho \cdot g \cdot \sin\theta \cdot q_i \cdot t^2}{\mu \cdot L \cdot A \cdot \phi^2} \qquad (2.4)$$

$$X_d = \frac{q_i \cdot t}{2 \cdot A \cdot \phi} - 4.94 \times 10^{-7} \frac{K \cdot \Delta\rho \cdot g \cdot \sin\theta \cdot q_i \cdot t^2}{\mu \cdot L \cdot A \cdot \phi^2} \qquad (2.5)$$

where: X_u = updip frontal location at t. (cm)

X_d = downdip frontal location at t. (cm)

q_i = injection rate. (cc/sec)

A = total cross-sectional area. (cm^2)

L = total length. (cm)

t = time. (sec)

ϕ = porosity. (fraction)

g = gravitational acceleration. (cm/sec^2)

K = permeability. (darcies)

$\Delta\rho$ = density difference. (gm/cc)

θ = dip angle. (degrees)

μ = viscosity. (cp)

Assumptions indigenous to development of equations 2.4 and 2.5 encompass:

(1) piston-like displacement

(2) fluids of small and constant compressibility

(3) homogeneous and isotropic porous medium of finite length

(4) breakthrough has not occurred in either direction.

The velocity in the system at (X_u, X_d) is found by taking the first derivative of equations 2.4 and 2.5 with respect to the time variable and rearranging terms to obtain:

$$\frac{dX_u}{dt} = \vec{V}_u = \frac{q_i}{2 \cdot A \cdot \phi} + 9.88 \times 10^{-7} \frac{K \cdot \Delta\rho \cdot g \cdot \sin\theta}{\mu \cdot \phi} \left[\frac{q_i \cdot t}{A \cdot L \cdot \phi}\right] \quad (2.6)$$

$$\frac{dX_d}{dt} = \vec{V}_d = \frac{q_i}{2 \cdot A \cdot \phi} - 9.88 \times 10^{-7} \frac{K \cdot \Delta\rho \cdot g \cdot \sin\theta}{\mu \cdot \phi} \left[\frac{q_i \cdot t}{A \cdot L \cdot \phi}\right] \quad (2.7)$$

The actual velocity of the fluid in a horizontal system or in a dipping system when there is no density difference between the injection and native fluids is the first term in both equations, $\frac{q_i}{2 \cdot A \cdot \phi}$. The second term, alike in each equation except for sign, is the velocity component attributable to dip. The portion of this term in brackets is a dimensionless quantity relating volume of injected fluid at any time to a given pore volume. This quantity is a weighting function which gives greater significance to the gravitational term as injection proceeds.

In modifying the linear equations (2.6 and 2.7) to describe a radial system, Painter[10] determined that the expression in brackets required an exponent in order to achieve agreement between his mathematical model and his experimental observations. Therefore, for a radial system, the total fluid velocity in the direction of dip (in this case the X-direction) is given by:

$$\vec{V}_x = \frac{q_i}{2 \cdot \pi \cdot h \cdot \phi} \left(\frac{x}{x^2 + y^2}\right) + 9.88 \times 10^{-7} \frac{K \cdot \Delta\rho \cdot g \cdot \sin\theta}{\mu \cdot \phi} \left[\frac{q_i \cdot t}{\pi \cdot r_e^2 \cdot h \cdot \phi}\right]^n \quad (2.8)$$

where: r_e = distance to nearest isopotential. (cm)

$\left[\frac{q_i \cdot t}{\pi \cdot r_e^2 \cdot h \cdot \phi}\right]^n$ = a ratio of the cumulative volume of injected fluid at any time to a given pore volume, dimensionless.

The radial velocity component attributable to dip is:

$$\vec{V}_g = 9.88 \times 10^{-7} \frac{K \cdot \Delta\rho \cdot g \cdot \sin\theta}{\mu \cdot \phi} \left[\frac{q_i \cdot t}{\pi \cdot r_e^2 \cdot h \cdot \phi}\right]^n \qquad (2.9)$$

Painter[10] experimentally verified the analytical solution developed for the linear case with a series of runs in a thin (0.50 cm), linear (10 cm by 140 cm) miniaquifer. He concluded that n = 1.0 for a linear system because all of the fluid movement is in a direction parallel to the boundaries. For a radial system he surmised that the exponent, n, differed from unity because of circulation of fluid around the periphery of the injected bubble and determined its value to be 0.17. This value was based on an analysis of data obtained from experimental runs in a thin, radial miniaquifer which was treated as a two-dimensional system. This miniaquifer was half of a circular system whose dimensions were 105 cm radius by 1.1 cm thick, bordered completely by a circular isopotential and containing one well in the center.

Painter's[10] initial attempt to determine a value for the exponent, n, was made by subtracting from the total velocity of the injected mass the component of velocity in

the X-direction attributable to injection. Using this technique, an order of magnitude number was obtained. This number was refined by a trial and error procedure to the value 0.17. Employing this value for n, the mathematical model predicted results which approximated those observed experimentally. This series of experimental runs involved injection of a volume of liquid at a predetermined rate into the radial miniaquifer after positioning the system at the desired angle. Tracings were made of the bubble configuration during migration.

To further substantiate the value of n of 0.17, Painter[10] made a series of 5 runs in which a "bubble" of known size was injected into the radial miniaquifer while it was horizontally oriented. The miniaquifer was then tilted to the desired angle and movement of the front of the injected fluid was observed and recorded by tracings. By measuring the elapsed time for each tracing, a velocity for each time increment was computed by dividing the change in position of the bubble center by the corresponding change in time. From these data an average velocity was calculated for the set of tracings for each run. Using the average velocity for each run, the slope of a log-log plot of equation (2.9) is the value of the exponent, n. Painter's[10] line of slope passing through the data points was 0.17 (see Figure 2.1). This further substantiated the value 0.17 determined from the radial displacements.

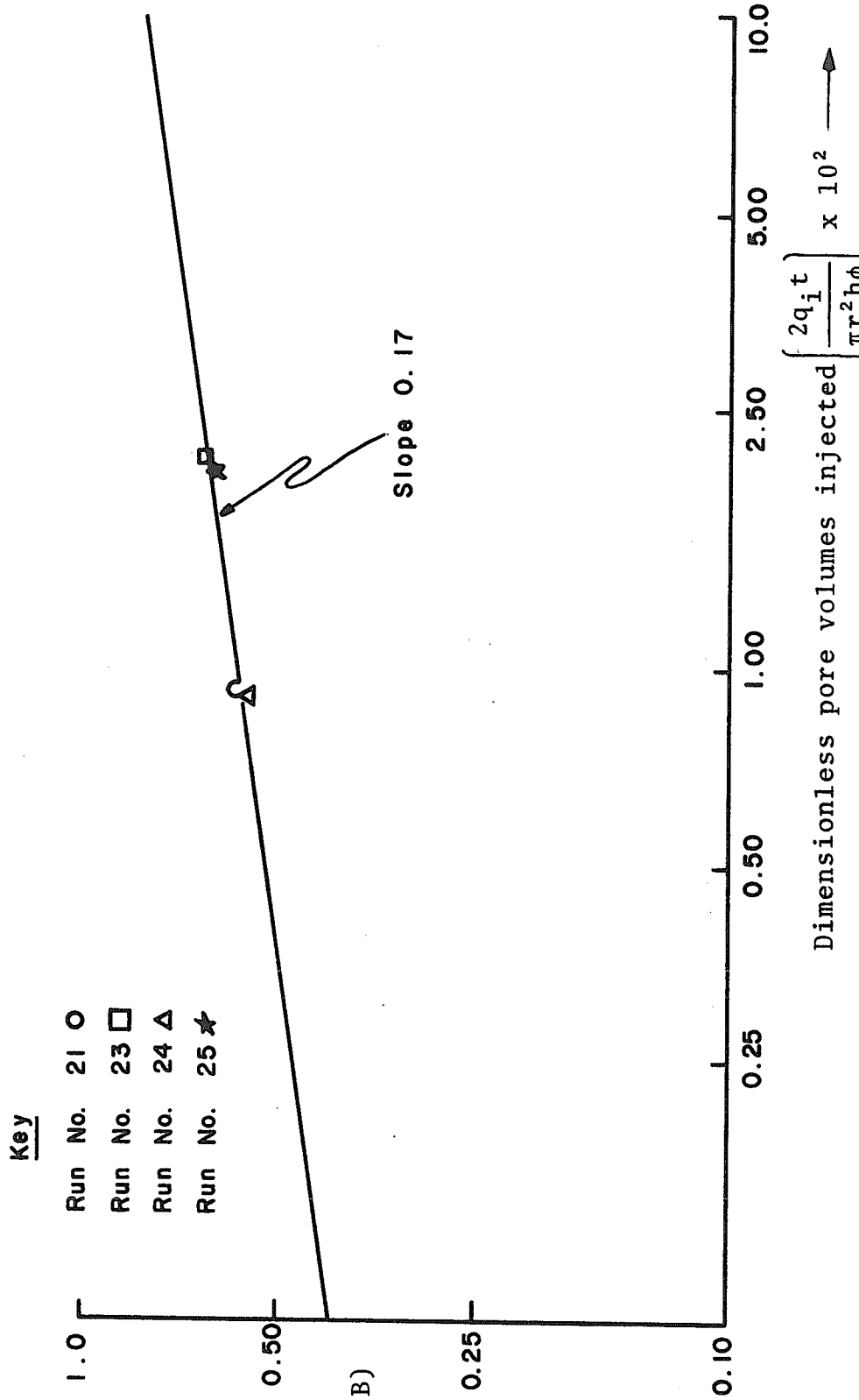

Figure 2.1. Graph of rearranged Equation (2.9) where n = 0.17. (After Painter[10])

2.5 Mathematical Models of Horizontal Three-Dimensional Systems

Kumar[8] developed a computer calculation procedure to estimate the recovery efficiency in a three-dimensional radial system. This program included the calculation of the mixed zone length and the horizontal projection of the interface due to gravity segregation.

To calculate the mixed zone due to dispersion and diffusion, Whitehead[13] used an idealized flow system during an injection half-cycle in which gravitational segregation was ignored (see Figure 2.2). In this system, as the injected fresh water displaces the native salt water, the mixing between the two fluids creates a transition zone in which the composition of either fluid will vary from 100 to 0 percent.

Assuming no mixing, R in Figure 2.2 is the radius of the injected fluid at any time, t. Therefore, the average value of C_n/C_o is 0.5 at radius R. In his computational procedure, the mixed zone length about any radius R and at any time t was calculated using the appropriate form of equation (2.2).

In calculating the projection of the interface due to gravitational segregation, Whitehead[13] used the following stepwise procedure:

(1) Let the fresh water be injected to a radius of R_{max} (see Figure 2.3). Note that only the 50 percent concentration lines, with gravitational segregation included, are considered.

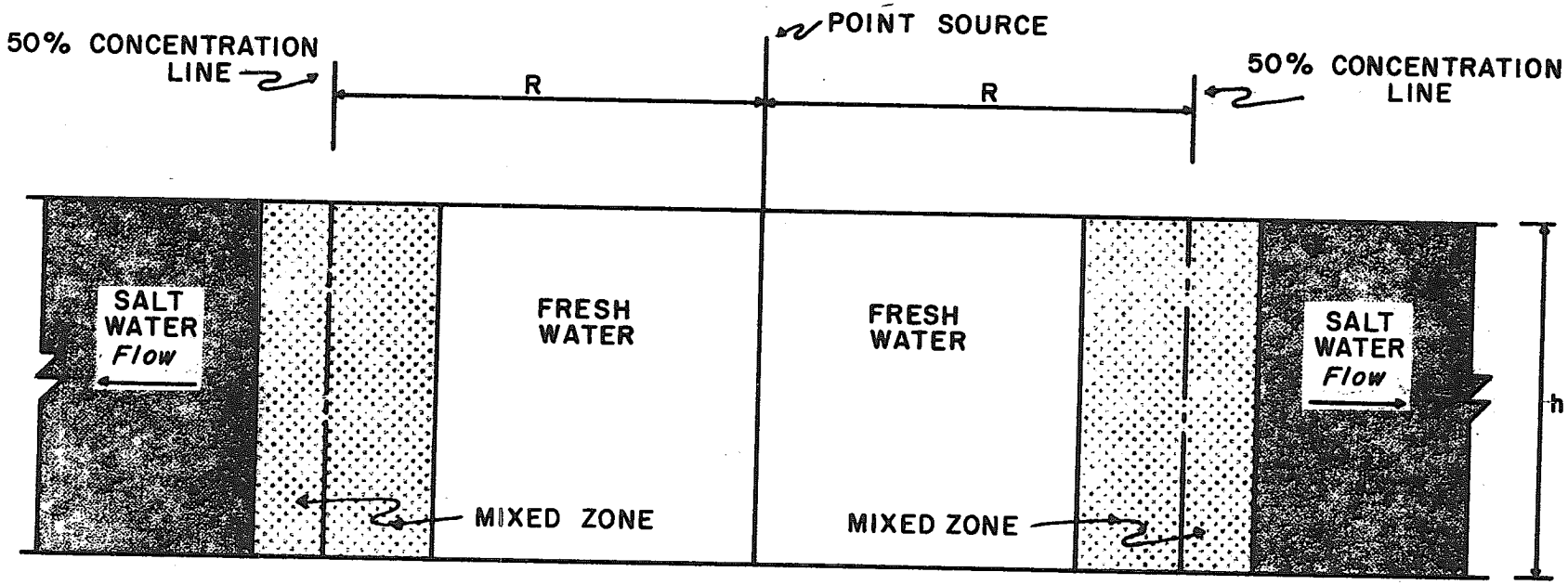

Figure 2.2. Schematic representation of the displacement process during an injection half-cycle. Gravitational segregation is ignored. (After Whitehead[13])

(2) Divide the distance R_{max} into equal intervals.

(3) Calculate the length of the mixed zone at the center of the first interval, C_1, by using the appropriate form of equation (2.2).

(4) This value of mixed zone length at C_1 is used to compute the value of the density gradient, S, which is assumed constant over the interval OR_1, by using the appropriate form of equation (2.2).

(5) The horizontal projection $(\overline{ZXL})_1$ at the end of the first interval is calculated using the value of S_1, the real time of travel, t_1, from 0 to R_1, and equation (2.3).

(6) For the second interval, R_1R_2, the mixed zone length is again computed at the center, C_2, of the interval. Since the mixed zone length at C_2 is greater than that at C_1, S_2 will be less than S_1.

(7) Assuming that the density gradient has been constant at a value of S_2 over the interval OR_2, a pseudo-time, t_1', is calculated which will give a horizontal projection at the end of the first interval that is equal to $(\overline{ZXL})_1$. Because S_1 is greater than S_2, the time t_1 will be less than the pseudo-time, t_1'.

(8) The horizontal projection $(\overline{ZXL})_2$ at the end of the second interval is calculated by adding the real time of travel from R_1 to R_2 to the pseudo-time to give a total time t_2. Using this technique the calculations for subsequent intervals are made.

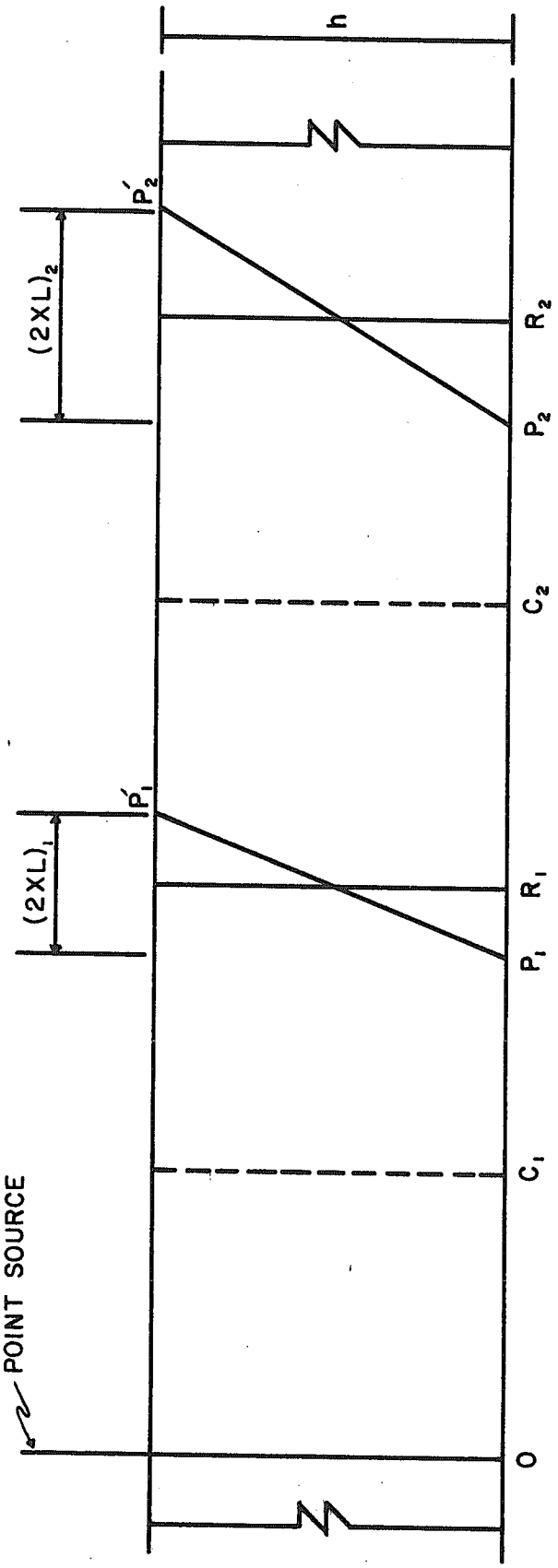

Figure 2.3. Schematic representation to illustrate the calculation of gravitational segregation before approximation to radial geometry. (after Whitehead[13])

The projection of the interface in the preceding treatment was calculated on the basis of a linear geometry. Whitehead[13] was able to apply these results obtained from a linear system to the radial system by use of a geometric correction.

Painter[10] developed a streamline tracking program which considered the injection well to be a point source in an infinite two-dimensional system. This program can track a maximum of fifty-five streamlines from the point source and gives a listing of the X and Y coordinates of each streamline for each time step. The time step is controlled by the choice of incremental distance traveled, ΔX. Dispersion was excluded by assuming piston-like displacement at the front. Painter[10] selected the value of the exponent, n, of equation (2.8) which best fit his experimental data. This value was based on an analysis of data obtained from experimental runs in a thin (1.1 cm thick), radial miniaquifer which was treated as a two-dimensional system. In his analysis, Painter actually traced the lower surface of the front of the injected bubble but calculated, due to his assumptions of a two-dimensional system and piston-like displacement, the midpoint between the upper and lower surface of the front. This discrepancy was due to the thinness of his miniaquifer which caused it to be translucent. Because of this only the lower surface of the bubble migration could be observed. This may explain the rather poor

agreement which he sometimes found between the calculated and observed frontal configuration. The discrepancy became progressively worse in the downdip direction where the effects of gravity segregation were more pronounced.

CHAPTER III

EXPERIMENTAL PROCEDURE

The experimental work consisted of the study of miscible displacements involving fluids of unequal density in a dipping miniature aquifer (miniaquifer). Radial displacements were measured to test the applicability of Painter's[10] results to a three-dimensional system.

The miniaquifer used in this investigation was built by W. R. Whitehead and consisted of an epoxy-sand mixture whose physical dimensions were 146 cm by 305 cm by 3.81 cm thick. A detailed description of the construction technique has been reported by Whitehead.[13] The miniaquifer was bordered on three sides by an isopotential and, due to symmetry, formed half of a rectangular system whose dimensions were 305 cm by 292 cm by 3.81 cm thick (see Fig. 3.1). Table 3.1 contains a listing of the miniaquifer's characteristics and Figure 3.2 is a photograph of the model with the monitoring equipment that was used during the experimental runs.

TABLE 3.1 Physical Characteristics of the Miniaquifer

Characteristic	Value
Porosity, ϕ	0.25, fraction
Permeability, K	5.57 darcies
Longitudinal dispersivity constant, α	0.02 cm

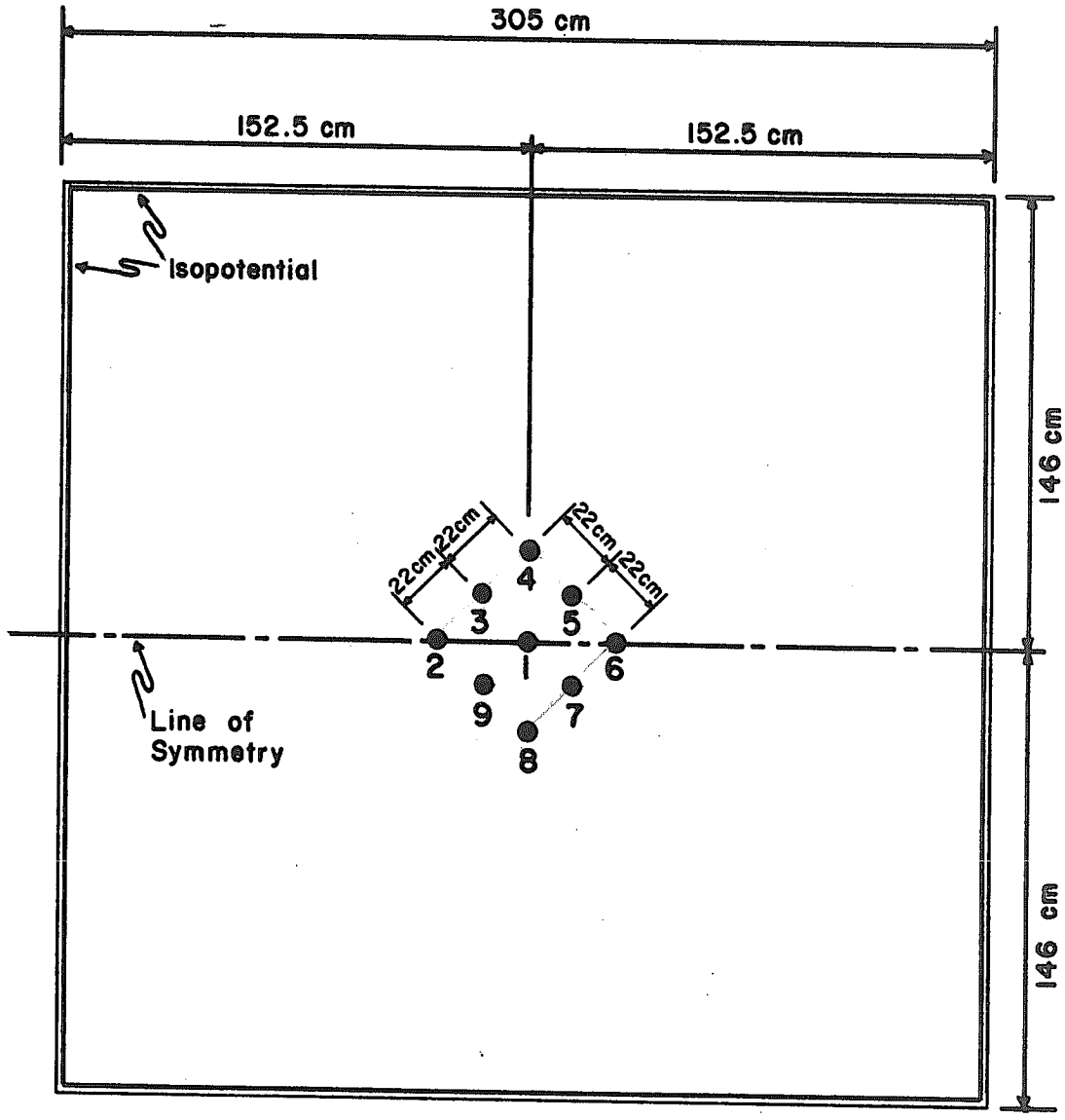

Figure 3.1. System represented by miniaquifer used in this investigation. (After Whitehead[13])

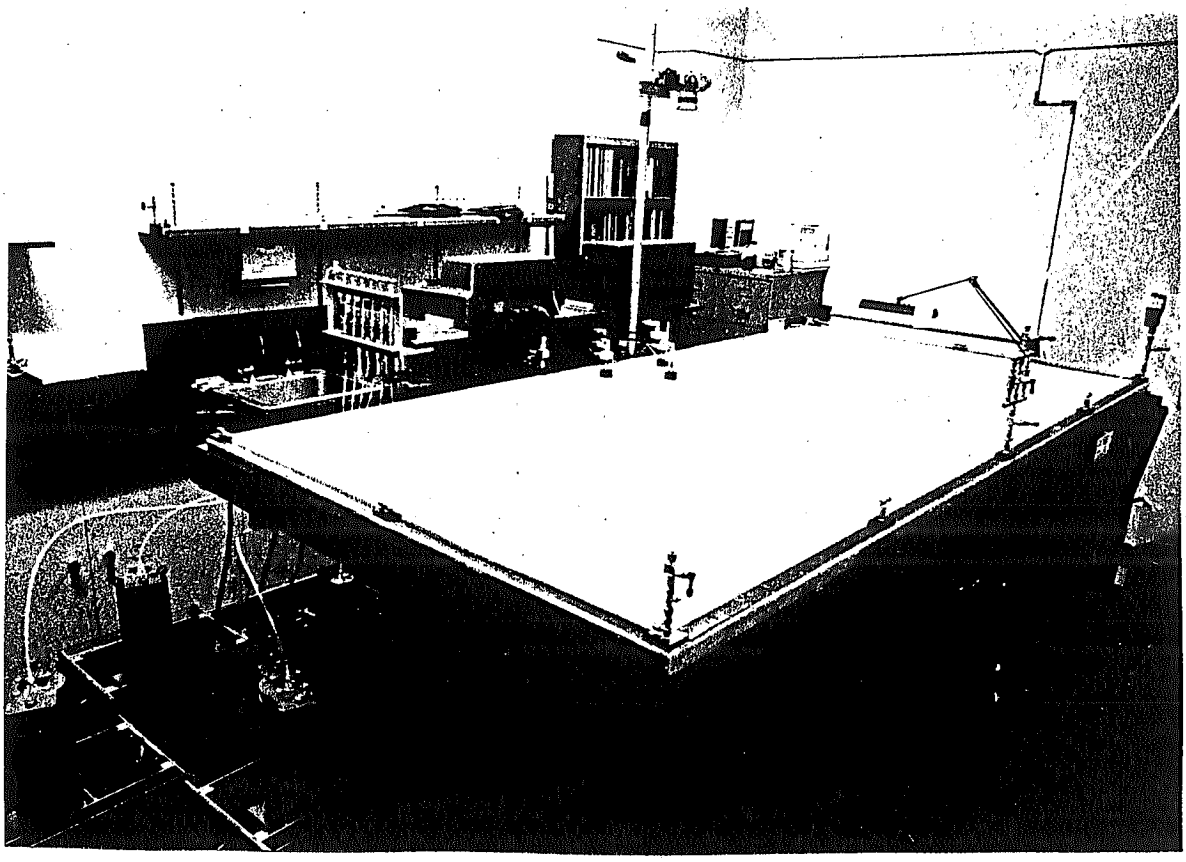

Figure 3-2. View of Miniaquifer, Pumps, and Instrumentation

After extensive tests Whitehead[13] found the mini-aquifer to be isotropic and homogeneous and determined that the maximum radius to which a bubble of fluid could be injected before the boundary effect was noticeable was 60 cm and that even at 100 cm, the effect was small. In the experimental runs conducted in the present investigation the largest bubble size injected had a radius of 50 cm so that the assumption of an isotropic, homogeneous, porous medium of infinite areal extent was valid.

Analog fluids which were miscible in all proportions were used in place of fresh and salt water in all of the experiments. The properties of the pure fluids used were measured by Whitehead[13] utilizing a Chainomatic gravitometer to measure the densities and an Ostwald viscometer to measure the viscosities. Table 3.2 lists these properties. The same equipment was employed to measure the properties of the various mixtures used in the experimental runs.

Analog fluids were used for several reasons:

(1) Better control of fluid properties is possible; for example, a wide range of density differences between native fluid and injected fluids can be obtained without changing the viscosity ratio;

(2) Introduction of water into a synthetic sandstone matrix similar to that used in the construction of the mini-aquifer sometimes inexplicably causes deterioration of the matrix.

TABLE 3.2 Properties of Pure Fluids Used in Experimental Runs

Fluid	Density at 22°C (gm/cc)	Viscosity at 22°C (cp)
[1]Naphtha	0.747	0.570
[2]Soltrol 170	0.771	2.504
[3]Carbon tetrachloride	1.590	0.992
[4]Iodobenzene	1.832	1.573

[1]Naphtha; V. M. & P.; Humble Oil and Refining Co.; Baton Rouge, La.

[2]Soltrol 170; Aliphatic Hydrocarbon; Phillips Petroleum Co.; Bartlesville, Okla.

[3]Carbon Tetrachloride; Technical Grade; F. H. Ross & Co.; Baton Rouge, La.

[4]Iodobenzene; Matheson, Coleman & Bell Mfg. Chemists; Norwood, Ohio.

The reservoir fluid in the miniaquifer was composed of a mixture of 43.5 percent soltrol, 53.2 percent naphtha, and 3.3 percent carbon tetrachloride by volume. The injection fluid consisted of a mixture of 45.0 percent soltrol and 55.0 percent naphtha by volume, to which varying amounts of carbon tetrachloride was added to yield a predetermined density difference between the reservoir and injection fluids. The specific mixture of 45.0 percent soltrol and 55.0 percent naphtha was found by Painter[10] to have the same viscosity as carbon tetrachloride, thus carbon tetrachloride could be added to the naphtha-soltrol mixture creating a

more dense fluid without changing the viscosity. The injected fluid also contained an oil-soluble red dye so that the progress of the injection fluid could be observed visually. In the runs in which the recovery efficiency was determined, 2.5 percent iodobenzene by volume was added to the injection fluid so that the dielectric constant of the injection fluid was appreciably different from that of the reservoir fluid. This difference was sensed by a capacitance cell which was connected to a chemical oscillometer. Whitehead[13] found that the concentration of reservoir fluid in the produced stream was linearly related to the millivolt signal that was generated when the oscillometer perceived a change in capacitance in its tank circuit. In this investigation, breakthrough was considered to have occurred when the concentration of reservoir fluid in the produced stream reached three percent. For convenience, in all of the runs the injection fluid was more dense than the reservoir fluid. This does not affect the experimental results since the recovery efficiencies obtained would be the same for a given set of conditions regardless of whether the injected fluid was more or less dense than the native fluid. The injected bubble's configuration and migration would be affected. For a given set of conditions, the injection of a less dense fluid would give exactly the opposite configuration and direction of migration in a dipping system when compared to the injection of a more dense fluid. Therefore, the

experimental results obtained are directly applicable to the injection of fresh water (less dense) into a salt water (more dense) aquifer provided the injected bubble's configuration and direction of migration are inverted.

After a mixture possessing the desired fluid properties was obtained, the injection fluid was loaded into large-barrel, constant-speed, positive-displacement pumps which were precisely machined and calibrated so that the rate of injection and production could be predetermined by selection of the proper gear ratio. The range for the injection and projection rates for each pump was defined by Whitehead[13] to be from 0.334×10^{-2} cc/min to 8.046 cc/min.

Two sets of experimental runs were made to determine the effect of dip on a miscible displacement process in a three-dimensional system. The first series of experimental runs which were made to determine an empirical value for the exponent, n, followed the same procedure as outlined by Painter[10] in his search for a value for n. First, the injection fluid was pumped into well no. 1 in the miniaquifer with the system horizontally oriented using four of the large-barrel pumps with each pump injecting at the rate of 8.046 cc/min for a maximum injection rate of 32.184 cc/min. This high rate was used in an attempt to minimize the inclination of the front due to gravity segregation. After injecting a predetermined volume, the four pumps were stopped and the miniaquifer was inclined to a pre-selected

dip angle. Only angles of 5°, 10°, 15°, and 20° were utilized due to the physical dimensions of the miniaquifer and its supporting stand. Frontal configurations of both the upper and lower surfaces of the injection bubble at selected time were traced on the miniaquifer and subsequently copied on tracing paper. After a sufficient number of tracings were made, the miniaquifer was returned to the horizontal position and the injected bubble was flushed out.

In the experimental runs to determine the recovery efficiency, the procedure was used with the following changes:

(1) The miniaquifer was placed at a 15° dip prior to the start of the run.

(2) The injected bubble was produced back at the same rate as that used for injection with the miniaquifer still at a slant.

(3) The injected fluid also contained 2.5 percent iodobenzene by volume so that its dielectric constant was appreciably different from that of the reservoir fluid. This is the same basic procedure that Painter[10] used in his series of runs to determine the recovery efficiency.

CHAPTER IV

ANALYSIS OF EXPERIMENTAL RESULTS

Two sets of experimental runs were made to determine the effect of dip on a miscible displacement process in a three-dimensional, isotropic, homogeneous, porous medium of assumed infinite areal extent. The first set of experimental runs (whose pertinent features are summarized in Table 4.1) was made to determine an empirical value for the exponent, n. The second set of runs was made to determine the recovery efficiency and to provide a standard against which a mathematical model could be compared.

In all of the runs in the first series, the frontal position of the upper surface of the bubble remained semicircular, decreased in radius with time, did not migrate, and at the end of each run appeared to be composed of a mixture of the injection and reservoir fluids (transition zone). Figure 4.1 exemplifies the frontal movement of the upper surface of the injected bubble for a typical run. (Remember that the injection fluid is of greater density than the native fluid.) The frontal position of the lower surface of the injected bubble began to migrate immediately in the direction of dip on the downdip side while on the updip side, the frontal position of the bubble in most runs

moved slightly updip before sliding downdip. In a few instances, the frontal position of the updip side of the bottom bubble surface began to slide immediately, but in all cases the updip side slipped only a minor distance in comparison to the downdip side. Figure 4.2 shows a typical pattern of bubble migration for the lower surface.

TABLE 4.1 Summary of Bubble Migration Study in a Dipping Porous Medium

Run No.	Dip Angle (degrees)	Density Difference (gm/cc)	Bubble Size (cc)	Mobility Ratio
1-1	10.0	0.0695	598.47	1.01
1-3	20.0	0.0695	598.47	1.01
3-2	15.0	0.0687	598.47	0.97
1-4	10.0	0.0695	1832.82	1.01
1-5	20.0	0.0695	1832.82	1.01
3-1	20.0	0.0687	3029.77	0.97
3-3	15.0	0.0687	3029.77	0.97
4-1	5.0	0.0740	2393.89	1.10
4-2	5.0	0.0740	598.47	1.10

In Figures 4.1 and 4.2 each tracing represents a three percent concentration level of the injection fluid at a given time. Utilizing data obtained by Whitehead[13] in his computer program, a plot of the radius of the 50 percent injection fluid concentration versus the 3 percent concentration radius was constructed (see Figure 4.3 and Table 4.2). From these data the radius of the 50 percent

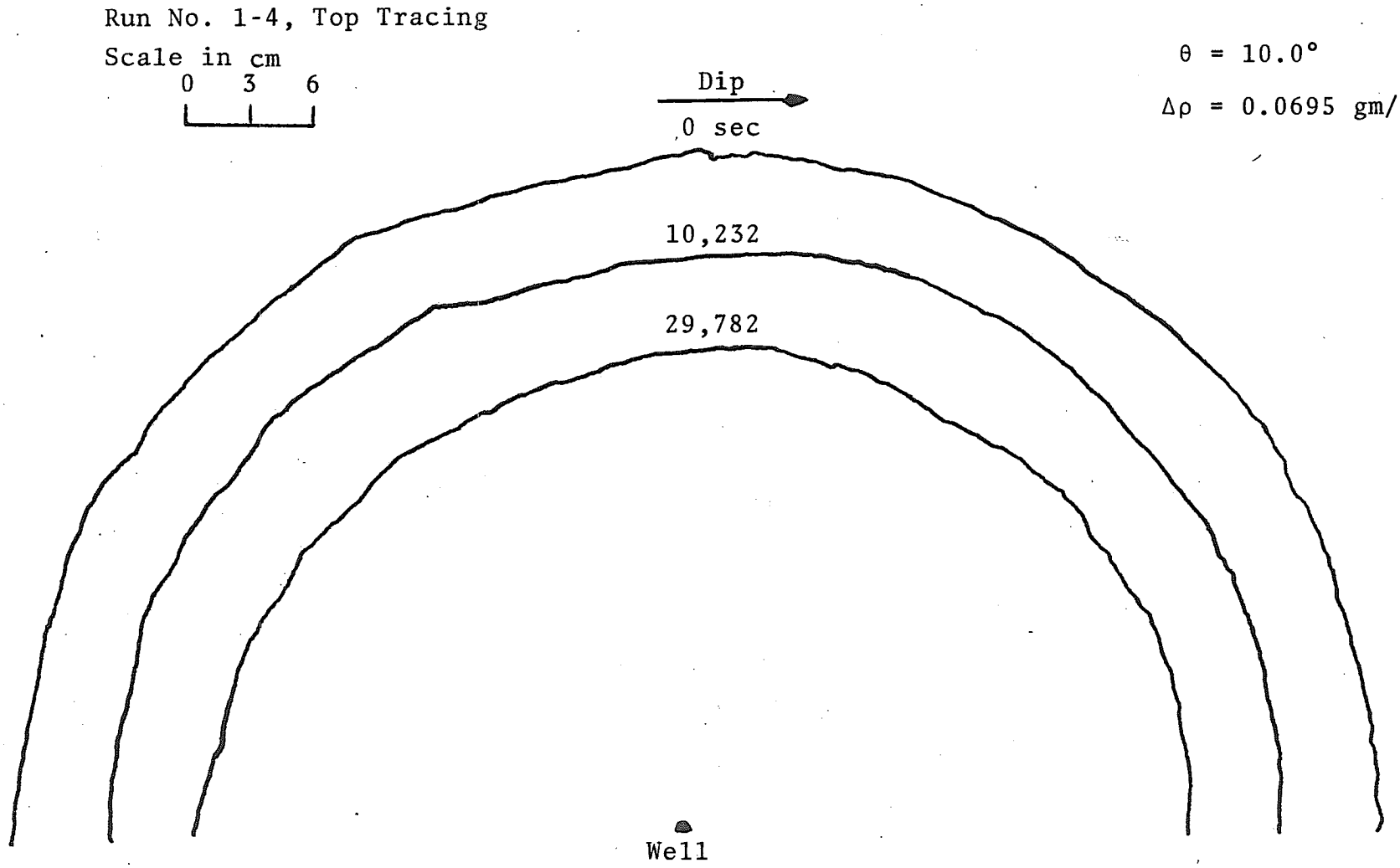

Figure 4.1. Selected Frontal Positions of the Upper Surface of the Bubble During a Typical Displacement

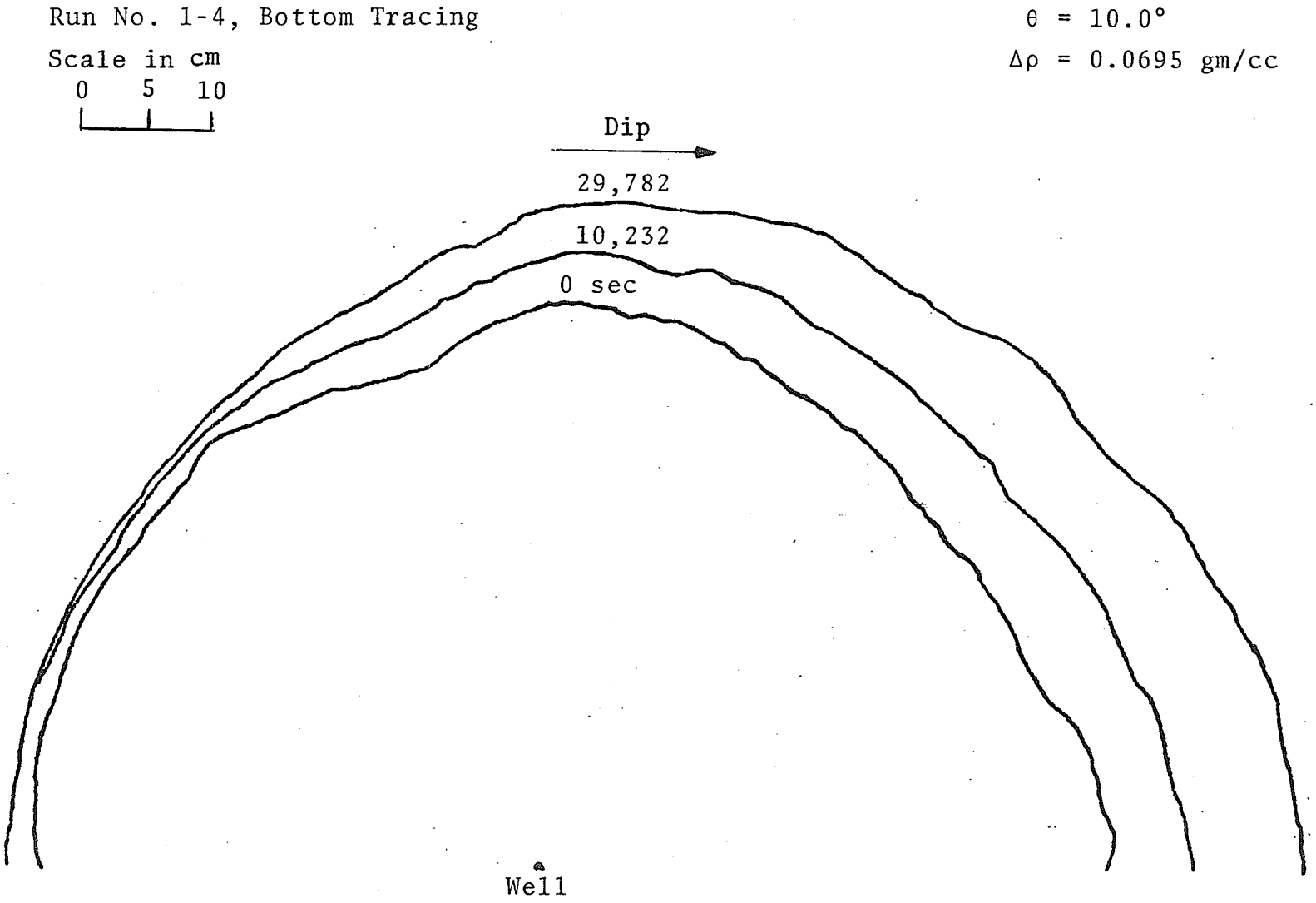

Figure 4-2. Selected Frontal Positions of the Lower Surface of the Bubble During a Typical Displacement

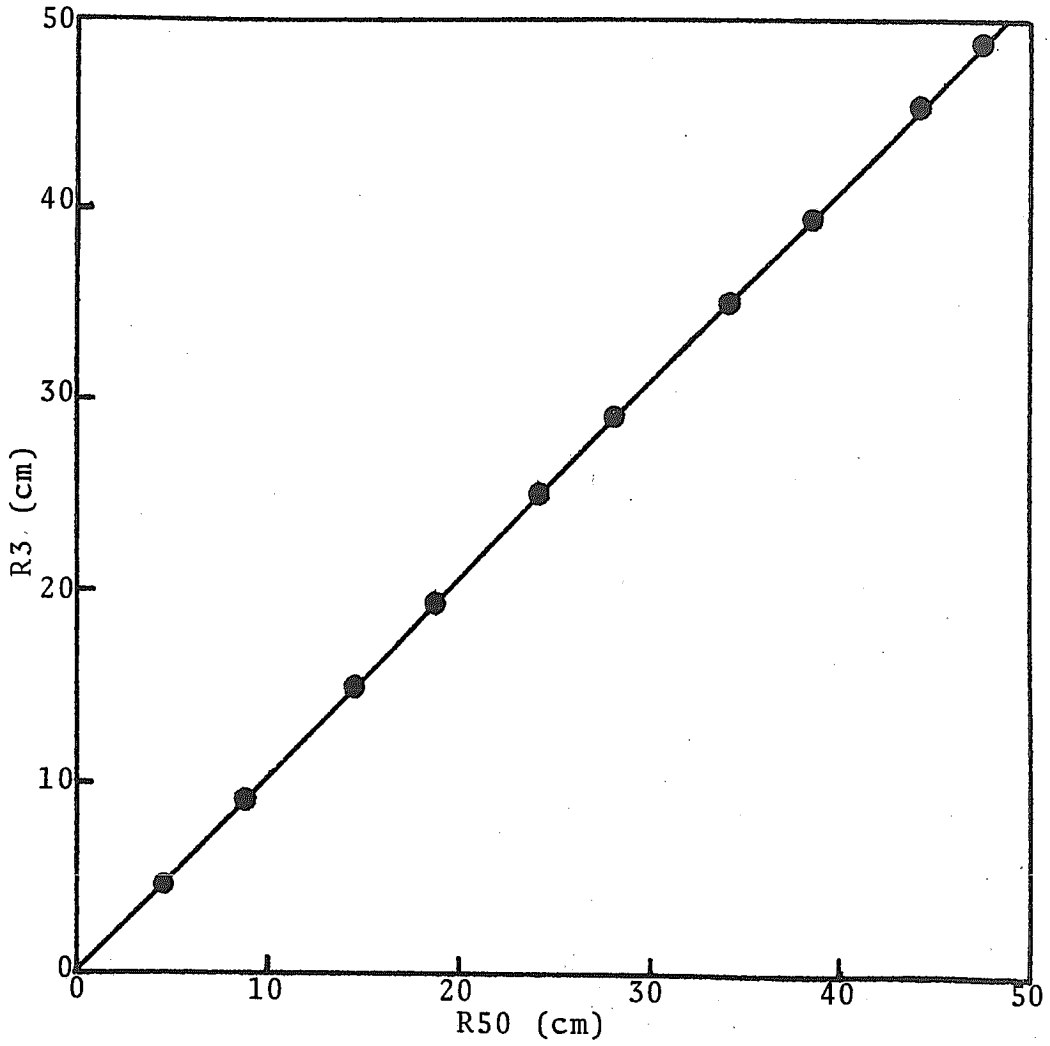

Figure 4-3. Plot of the Radius of the 3% Concentration Level (R3), versus the radius of the 50% Concentration Level (R50).

concentration level for each tracing was plotted. Appendix C contains tracings of the frontal migration of the lower surface of the bubble for each run, and Appendix D, the upper surface migration. Utilizing this information, the position of the bubble center for each 50 percent concentration level was calculated independently for both the upper and lower surfaces of the injected bubble for each run. By having previously measured the time after dip for each tracing, a velocity for each increment was computed by dividing the change in position of the bubble center by the corresponding change in time. From these data an average velocity was calculated for both the top and bottom set of tracings for each run. Appendix A comprises the data and calculations for the frontal movement of the lower surface of the injected bubble, and Appendix B, the upper surface. The average velocity for each group of data was divided by the factor, $9.88 \times 10^{-7} \frac{K \cdot \Delta\rho \cdot g \cdot \sin\theta}{\mu \cdot \phi}$, and plotted versus the dimensionless pore volume injected, $\frac{q_i \cdot t}{\pi \cdot r_e^2 \cdot h \cdot \phi}$, for each run on log-log graph paper. From these graphs an empirical value of the exponent n for both the top and bottom sets of data was obtained from the following analysis.

$$V_g = 9.88 \times 10^{-7} \frac{K \cdot \Delta\rho \cdot g \cdot \sin\theta}{\mu \cdot \phi} \left[\frac{q_i \cdot t}{\pi \cdot r_e^2 \cdot h \cdot \phi} \right]^n$$

Let $B = 9.88 \times 10^{-7} \frac{K \cdot \Delta\rho \cdot g \cdot \sin\theta}{\mu \cdot \phi}$

Therefore: $$V_g = B\left[\frac{q_i \cdot t}{\pi \cdot r_e^2 \cdot h \cdot \phi}\right]^n$$

And $$\frac{V_g}{B} = \left[\frac{q_i \cdot t}{\pi \cdot r_e^2 \cdot h \cdot \phi}\right]^n$$

Taking the log of both sides gives:

$$\log\left[\frac{V_g}{B}\right] = n \log\left[\frac{q_i \cdot t}{\pi \cdot r_e^2 \cdot h \cdot \phi}\right]$$

so that the exponent n becomes the slope of the curve when plotted on log-log paper.

TABLE 4.2. Comparison of the Radius of the 3% Concentration Level (R3), to the Radius of the 50% Level (R50), in cm

Increment	R3	R50	Increment	R3	R50
1	0.7	0.5	29	29.7	28.5
3	2.9	2.5	31	31.7	30.5
5	5.0	4.5	33	33.8	32.5
7	7.1	6.5	35	35.8	34.5
9	9.2	8.5	37	37.8	36.5
11	11.2	10.5	39	39.9	38.5
13	13.3	12.5	41	41.9	40.5
15	15.4	14.5	43	44.0	42.5
17	17.4	16.5	45	46.0	44.5
19	19.5	18.5	47	48.0	46.5
21	21.5	20.5	49	50.0	48.5
23	23.6	22.5	51	52.1	50.5
25	25.6	24.5	53	54.1	52.5
27	27.6	26.5	55	56.1	54.5

Tables 4.3 and 4.4 contain a listing of the pertinent information procured and Figures 4.4, 4.5, 4.6, and 4.7 comprise the curves. Table 4.5 is a comparison of the exponent n for the lower surface of the bubble migration to the dip of the system and shows that n is a function of dip. Figure 4.8 is a plot of Table 4.5 in rectangular coordinates. [Note that the exponent, n, may also be a function of aquifer thickness. However, this hypothesis can only be tested by using a miniaquifer of greater thickness.] The dashed line in Figure 4.8 is a theoretical approximation of the shape that the curve might take as it approaches zero. This approximation is based on the following reasons:

(1) The average velocity of the lower surface in the runs with an aquifer dip of 5 degrees was so low compared to all the other runs that a greater opportunity for experimental error existed;

(2) Many of nature's phenomena can be represented by an S-shaped curve. For example, the concentration profiles used in computing the longitudinal dispersivity coefficient formed an S-shaped curve when plotted.[13]

For the upper surface of the bubble movement the value of n was -0.0218 but due to the fluctuations in the data (see Table 4.4) the value obtained for n was considered within the realm of experimental error and therefore assumed to be 0.0.

TABLE 4.3

Summary of Bubble Migration Data Obtained from Evaluation of Tracings from the Lower Surface of the Miniaquifer

Run	Injection Radius (cm)	Dip	Average Velocity (cm/sec)	$\overline{V}_g/B$	$(P.V.)_D$
1-1	20	10°	2.06×10^{-4}	0.6658	1.929×10^{-2}
1-3	20	20°	3.545×10^{-4}	0.5780	1.929×10^{-2}
3-2	20	15°	2.376×10^{-4}	0.5706	1.929×10^{-2}
1-4	35	10°	2.218×10^{-4}	0.7160	5.904×10^{-2}
1-5	35	20°	4.175×10^{-4}	0.681	5.904×10^{-2}
3-1	45	20°	3.999×10^{-4}	0.7270	9.765×10^{-2}
3-3	45	15°	2.944×10^{-4}	0.7069	9.765×10^{-2}
4-1	40	5°	0.8460×10^{-4}	0.532	7.72×10^{-2}
4-2	20	5°	0.9148×10^{-4}	0.5755	1.929×10^{-2}

TABLE 4.4 Summary of Bubble Migration Data Obtained from Evaluation of Tracings from the Upper Surface of the Miniaquifer

Run No.	Injection Radius (cm)	Dip	Velocity (cm/sec)	$\overline{V}_g/B$	$(P.V.)_D$
1-1	20	10°	-0.085×10^{-4}	-0.02745	1.929×10^{-2}
1-3	20	20°	0.4977×10^{-4}	0.08162	1.929×10^{-2}
3-2	20	15°	0.5309×10^{-4}	0.1275	1.929×10^{-2}
1-4	35	10°	-0.00722×10^{-4}	-0.00233	5.904×10^{-2}
1-5	35	20°	0.647×10^{-4}	0.1061	5.904×10^{-2}
3-1	45	20°	0.221×10^{-4}	0.0402	9.765×10^{-2}
3-3	45	15°	-0.1872×10^{-4}	-0.04495	9.765×10^{-2}

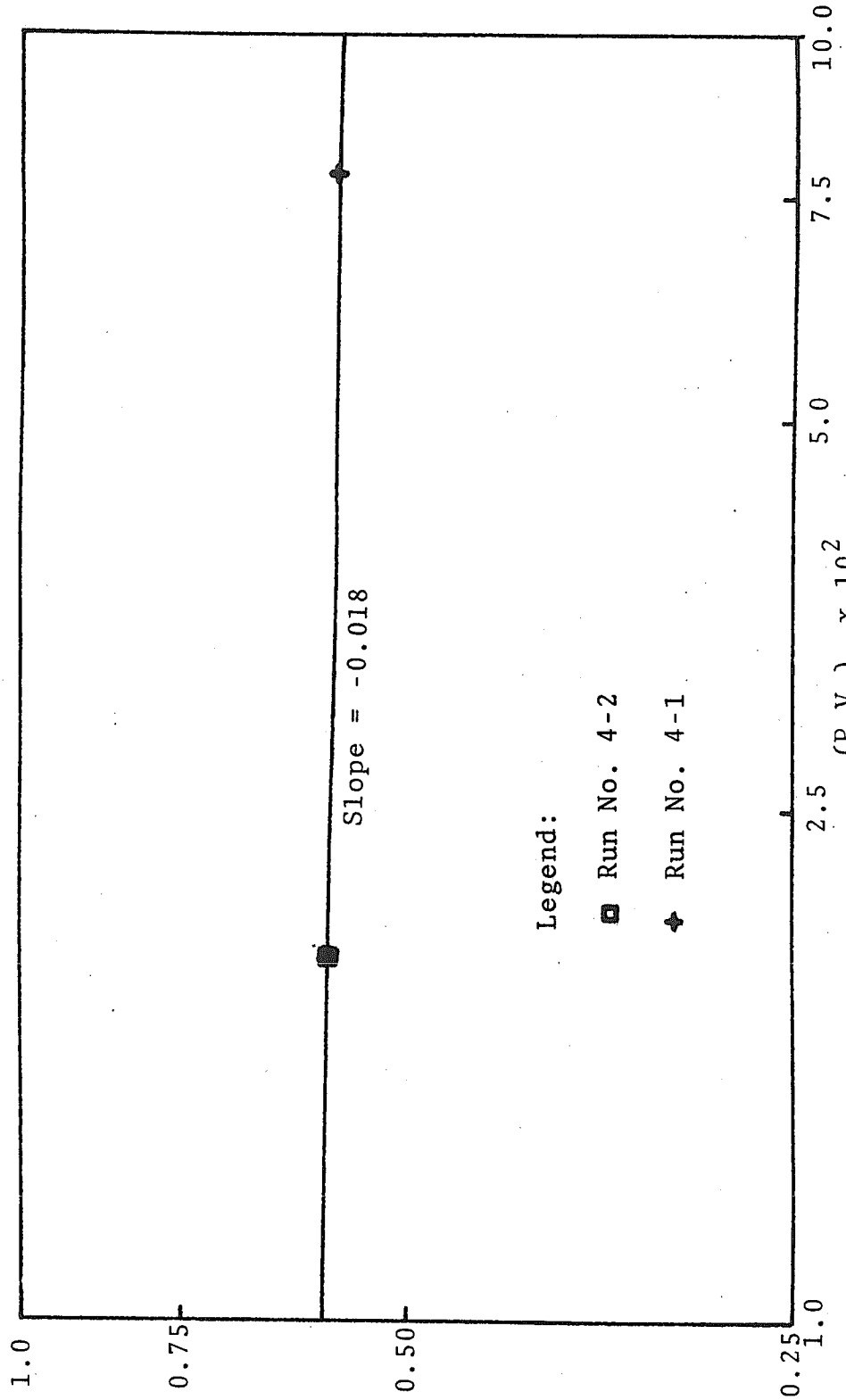

Figure 4-4. Plot of Data from Bottom Tracings for Runs with a Dip of 5°

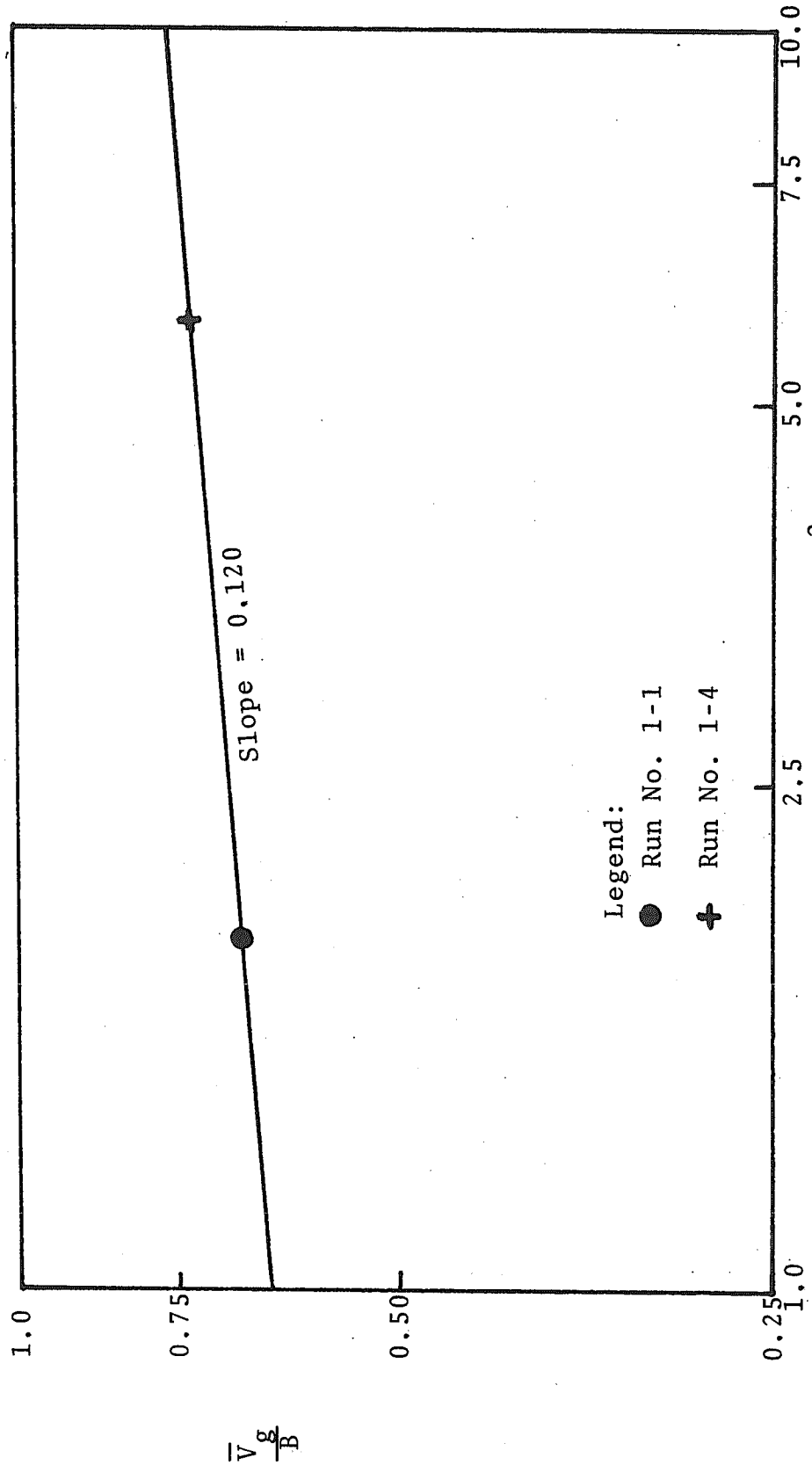

Figure 4-5. Plot of Data from Bottom Tracings for Runs with a Dip of 10°

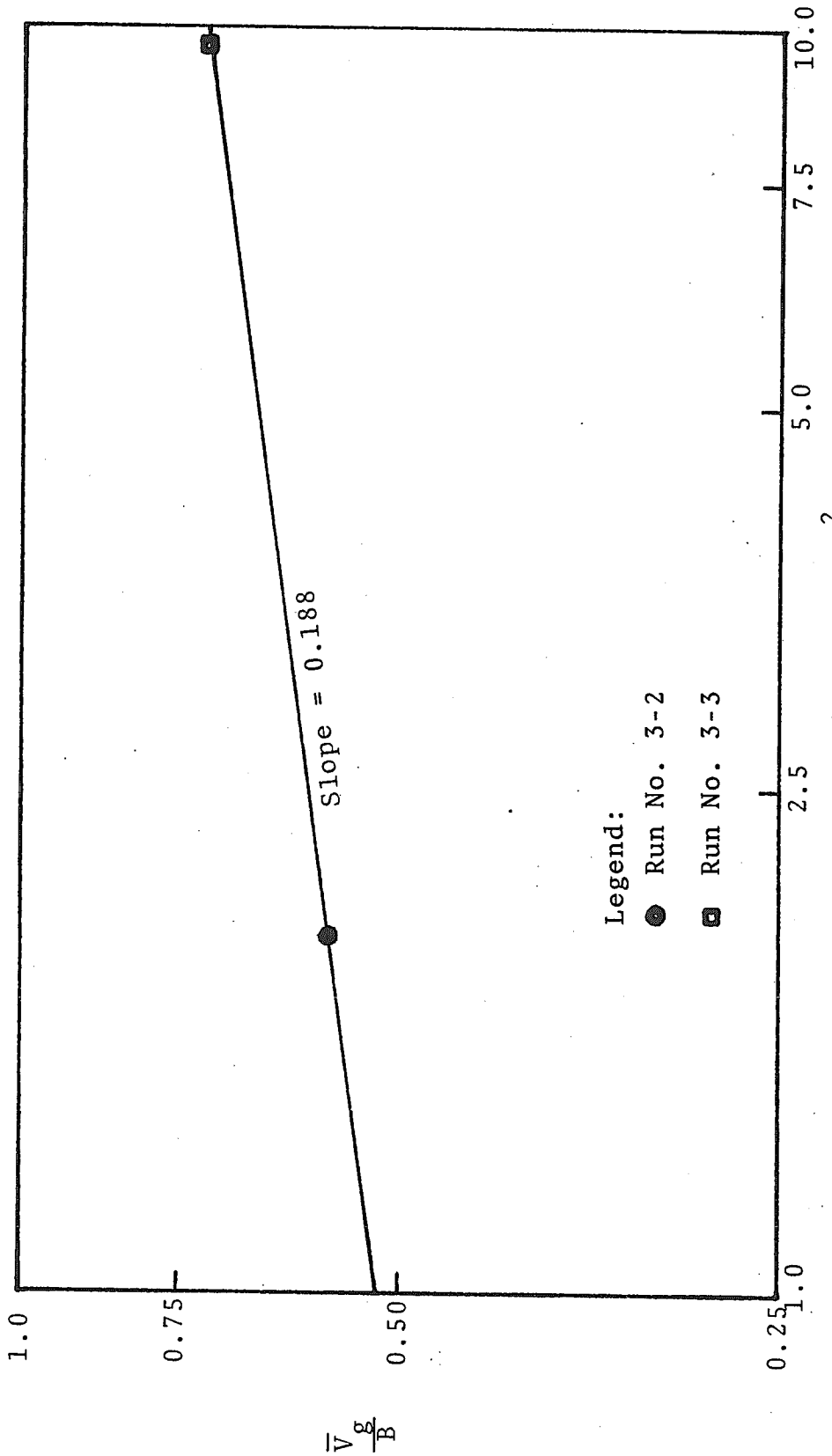

Figure 4-6. Plot of Data from Bottom Tracings for Runs with a Dip of 15°

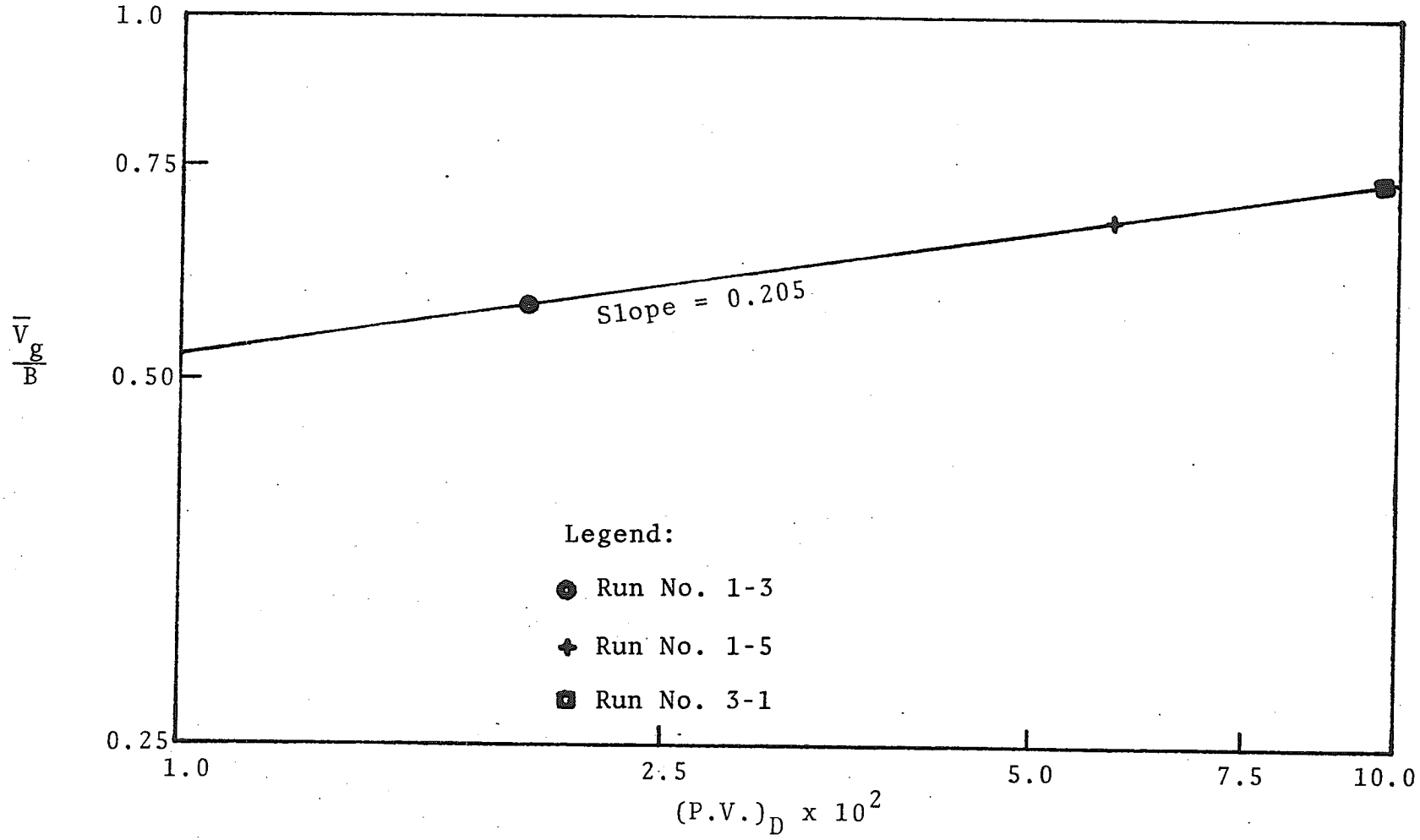

Figure 4-7. Plot of Data from Bottom Tracings for Runs with a Dip of 20°

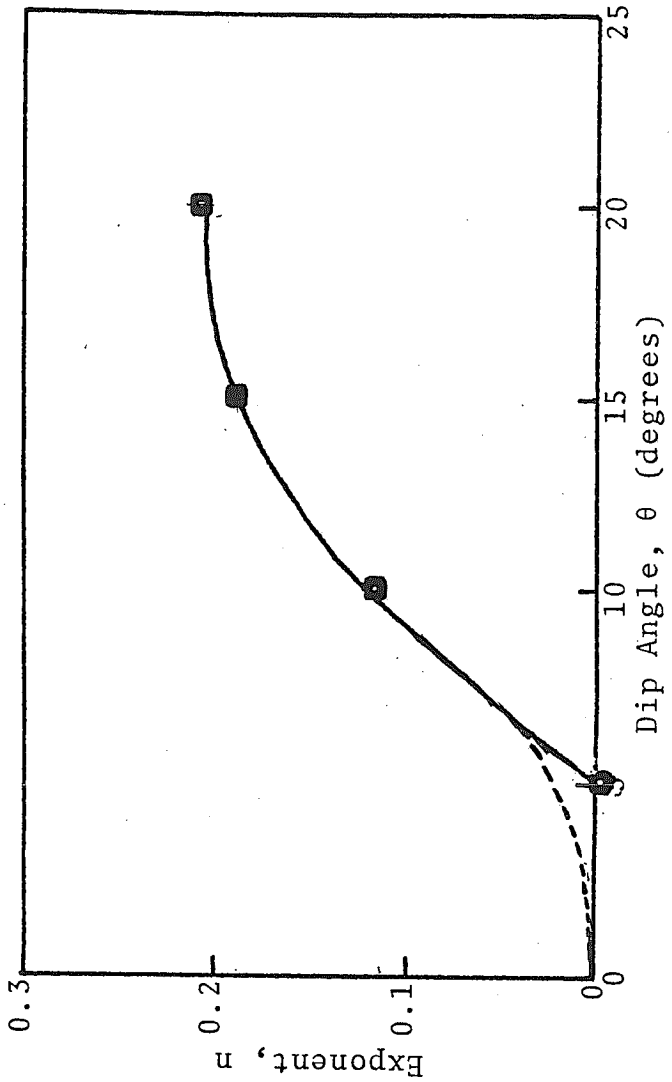

Figure 4-8. Plot of Exponent, n, versus Dip Angle, θ for tracings of the lower surface

TABLE 4.5 Relationship Between Dip and the Value of the Exponent n for the Lower Surface of the Bubble

Dip (degrees)	Exponent, n (fraction)
5.0	-.018
10.0	0.12
15.0	0.188
20.0	0.205

In runs 2-1 and 2-2 the recovery efficiency was calculated for a dipping system and the results compared in Table 4.6 with the recovery efficiencies expected in similar horizontal situations. Also included in the comparison are two runs made by Whitehead.[13] Table 4.6 indicates that the recovery efficiency is lower in a dipping system than in a similar horizontal case and that the reduction increases as storage time lengthens. Comparable results were obtained by Painter[10] for the two-dimensional case.

In developing a computer program to match the configuration of the lower surface of an injected bubble for an injection cycle, selected portions of Whitehead's[13] and Painter's[10] programs were combined. Originally, only Painter's[10] program was used with only one adaptation. This change involved letting the exponent, n, from the computational procedure vary with the dip angle. This manipulation improved the accuracy but the error induced on the downdip side of the frontal migration was still too large. The poor agreement in the downdip direction was a result of attempting to describe a three-dimensional system by two-dimensional

TABLE 4.6

Comparison of Recovery Efficiency in a Dipping System to a Horizontal System

Run No.	Dip Angle (degrees)	Density Difference (gm/cc)	Injection and Production Rates (cc/min)	Injection Time (sec)	Storage Time (sec)	Recovery Efficiency (%)
2-1	15.0	0.06638	32.184	6,973	0.0	66.60
2-1*	0.0	0.06638	32.184	6,973	0.0	69.17
2-2	15.0	0.06638	32.184	5,350	5350	41.87
2-2*	0.0	0.06638	32.184	5,530	5350	57.81
2	15.0	0.4286	3.658	15,100	0.0	11.0
1	0.0	0.4286	3.658	15,100	0.0	15.0

*Horizontal runs obtained by incorporating similar data into Whitehead's[13] computer program.

analysis. A two-dimensional approach assumes piston-like displacement of the front and therefore excludes both gravity laydown of the front and dispersion. To alleviate this problem a pseudo-injection rate was obtained in the following manner:

(1) The identical parameters for each run, excluding dip, used in Painter's[10] program was read into Whitehead's[13] program for an injection half-cycle because of its inclusion of gravity segregation and dispersion. Dip was excluded because Whitehead's program was only for the horizontal system. By assuming a small value for thickness later, the difference between gravity laydown of the front and dispersion in a horizontal system as compared to a dipping system was minimized.

(2) From the computer print-out of the RU50 values, which are the radii from the wellbore to the 50 percent concentration levels for the top surface of the bubble (see Figure 4.10), the radius corresponding to the maximum injection time was obtained. Note that Whitehead's[13] top surface of the bubble is the same as the bottom surface in this investigation. This is because his program is based on the injection of a less dense fluid instead of a more dense fluid as used in this investigation.

(3) An arbitrarily small value for thickness was chosen.

(4) The volume for a semi-radial system was

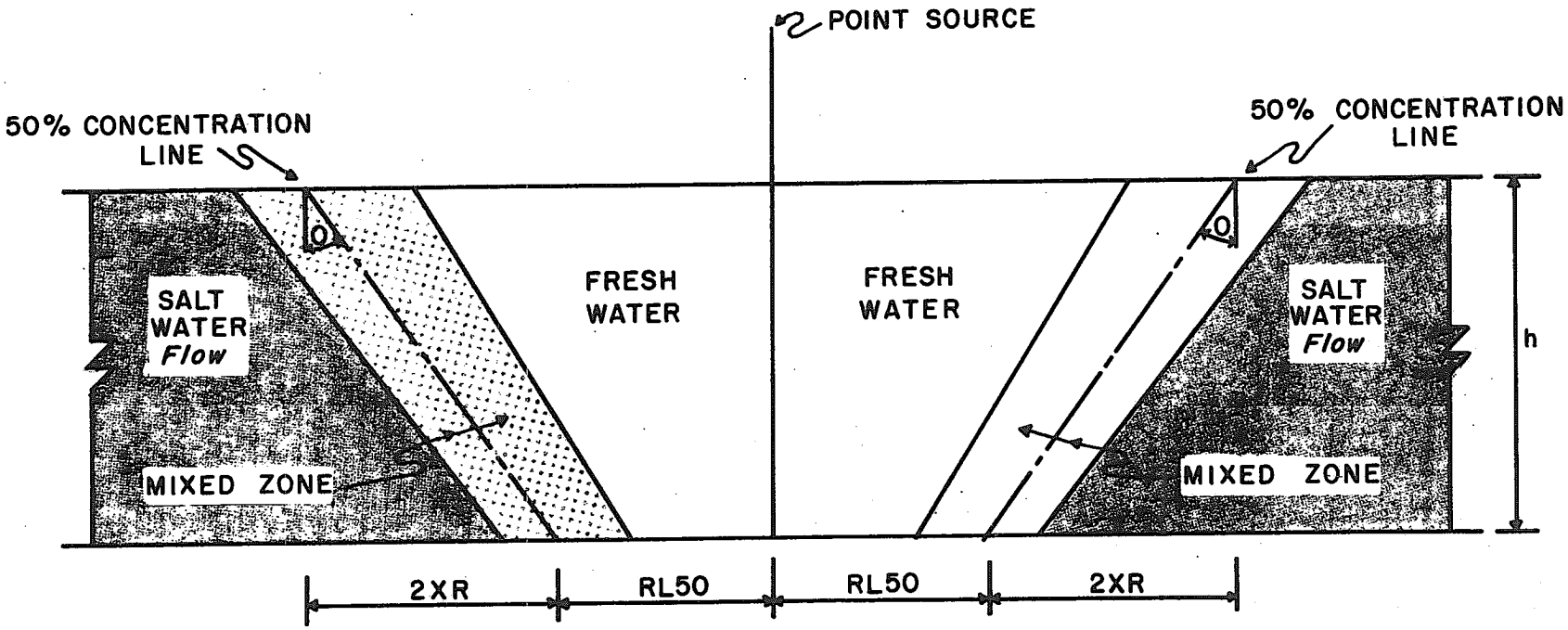

Figure 4.9. Schematic representation of the displacement process during an injection half-cycle. Both mixing and gravitational segregation are included. (After Whitehead[13])

determined by incorporating the above values for thickness and radius into the equation:

$$\text{volume} = \frac{\pi \cdot r^2 \cdot h \cdot \phi}{2}$$

where:

r = radius, cm

h = thickness, cm

ϕ = porosity, %

(5) The pseudo-injection rate was obtained by dividing the volume by the appropriate injection time.

This new injection rate and the new value for thickness were incorporated into Painter's[10] program and provided excellent agreement with the experimental tracings (see Figure 4.11). Painter's[10] program actually tracked a maximum of fifty-five streamlines from the point source and gave a listing of the x and y coordinates of each streamline for each time step. (The time steps are specified by the programmer.) By connecting the data point from each x and y coordinate of each streamline for a given time to one another, a configuration of the frontal migration of the injected bubble was drawn for that particular value of time. Time in both the computer program and experimental runs was measured from the initiation of injection. This process is repeated to obtain the frontal configurations for other time intervals. The accuracy of the agreement was further improved by using a specific pseudo-injection rate for each tracing. These rates were obtained using the same

Run No. 2-1, Bottom Tracing

Injection = ——— observed experimental configuration
Predicted = - - - - -
Predicted using specific pseudo-injection rate = + + + + + +

θ = 15.0°
$\Delta\rho$ = 0.0664 gm/cc
q = 32.184 cc/min

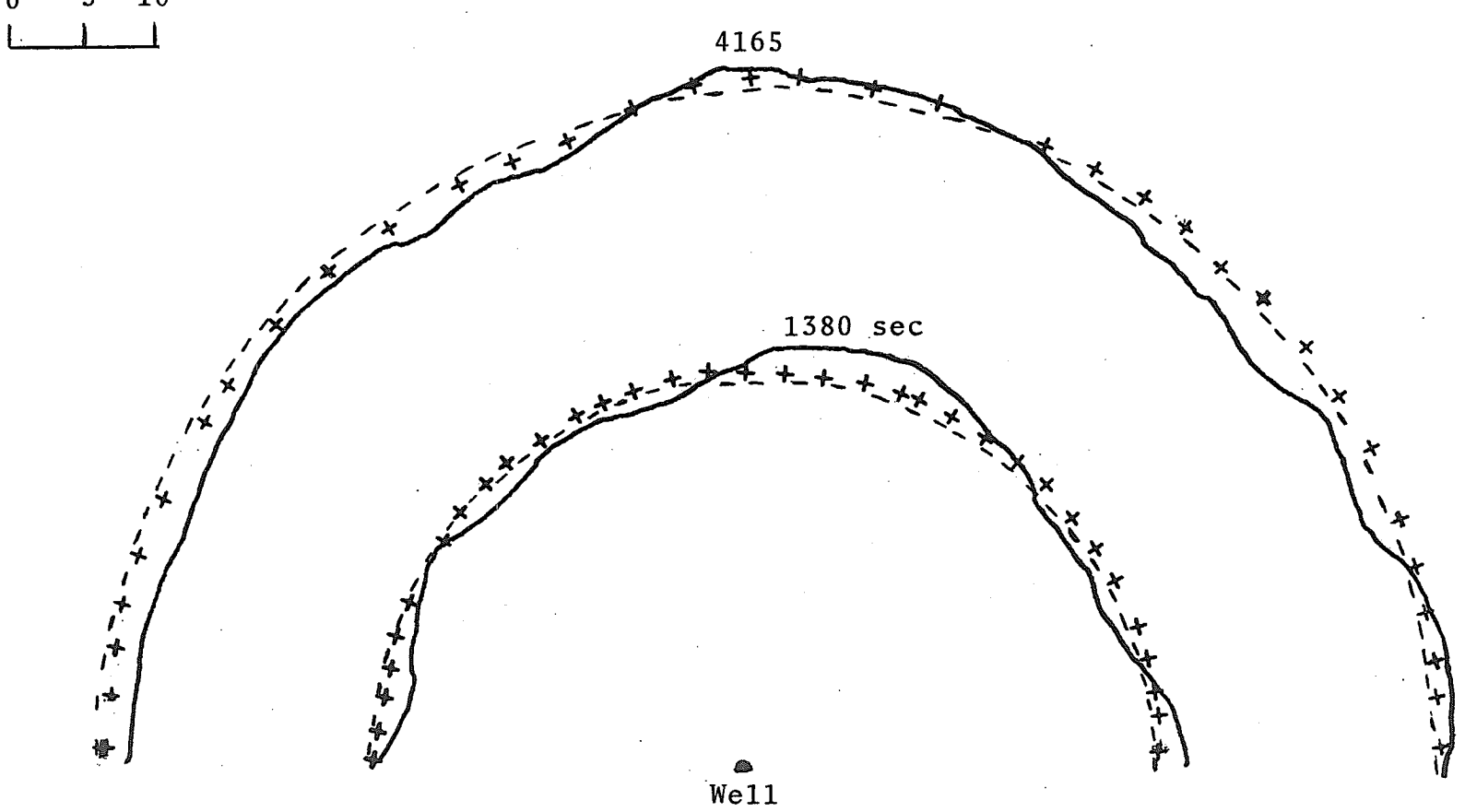

Figure 4.10. Comparison of Experimental Run to Computer Model

procedure except that the maximum radius of injection was replaced by the radius which corresponded to the time for each tracing.

The same basic procedure should work for predicting frontal configurations during a production half-cycle. However, such comparisons were not made in the present study.

CHAPTER V

APPLICATION OF RESULTS

Prediction of the configuration and migration of an injected bubble of fluid in a dipping aquifer under field conditions must be done with utmost caution since the calculation procedure in Chapter IV requires that a radius, r_e, at which the potential remains unaltered during the period of interest, be stipulated. Furthermore, the assignment of a realistic value for r_e is of great importance to the mathematical model. This is because the radial velocity component attributable to dip, $\vec{V}_g$, is dependent on the ratio of volume injected to total system pore volume out to this radius. This can be more readily seen by reviewing Equation (2.9):

$$\vec{V}_g = 9.88 \times 10^{-7} \frac{K \cdot \Delta\rho \cdot g \cdot \sin\theta}{\mu \cdot \phi} \left[\frac{q_i \cdot t}{\pi \cdot r_e^2 \cdot h \cdot \phi} \right]^n$$

During this investigation, the maximum point of experimental frontal advance was kept to approximately one-third the distance to the nearest isopotential.

Had the radius r_e been chosen in a different manner in this investigation, the correlations would undoubtedly have produced other values for the exponent n than those

proposed. Therefore, the reliability to be expected in applying these results to field cases will not be known until additional studies have been conducted in which r_e is treated as a variable. It is proposed, without experimental verification, that the results might be applied in the field by assuming r_e to be three times the radius of the maximum bubble size to be injected. This assumes that the aquifer will not be appreciably disturbed by the injected bubble beyond such a radius. It is anticipated that future study may suggest a stepwise procedure in which r_e is treated as a function of the total volume that has been injected at a given time.

The reader is again reminded that the exponent, n, may be a function of aquifer thickness or, more likely, a ratio involving aquifer thickness and bubble size. This possibility has not yet been investigated. Until further studies have been made, the results presented herein should be treated as preliminary and used primarily as a qualitative guide when applied to field situations.

CHAPTER VI

CONCLUSIONS AND RECOMMENDATIONS

6.1 Conclusions

On the basis of this investigation, the following conclusions are drawn with regard to storage of fresh water in a dipping saline aquifer. Note that this case involves injection of a less dense fluid into a more dense reservoir fluid. When applied to the injection of a more dense fluid, one would obtain exactly the reverse configuration and direction of migration in a dipping system. The recovery efficiencies observed would be the same for a given set of conditions regardless of whether the injected fluid was more or less dense than the native fluid. The conclusions are:

(1) The configurations of the lower surface of the injected fresh water bubble at successive times will appear as a series of concentric circles whose centers of mass will remain coincident with the point of injection.

(2) The configuration of the upper surface of the injected bubble will appear initially as a series of concentric circles whose centers of mass will be displaced updip due to the gravity gradient.

(3) The frontal movement of the 50 percent

concentration line of the upper surface of the injected bubble in a three-dimensional dipping system with an isopotential at a radius three times the maximum radius of frontal progression, can be approximated by combining an empirically weighted term,

$$9.88 \times 10^{-7} \frac{K \cdot \Delta\rho \cdot g \cdot \sin\theta}{\mu \cdot \phi} \left[\frac{q_i \cdot t}{\pi \cdot r_e^2 \cdot h \cdot \phi} \right]^n$$

with the steady-state solution to the diffusivity equation.

(4) The velocity due to dip remained zero for the lower surface of the injected bubble and increased for the upper surface as the dip angle became progressively larger and also as the size of the injected bubble increased.

(5) The recovery efficiency will be lower in a dipping system than in a similar horizontal situation. This reduction increases with an increase in storage time because the injected bubble continues to migrate after injection is completed.

(6) An empirical correlation for the velocity of migration of a bubble of injected fluid has been obtained for dip angles of less than five degrees. This velocity is directly proportional to the sine of the dip angle.

6.2 Recommendations

Recommendations for further study on the storage of fresh water in saline aquifers are:

(1) Determine the effect of aquifer thickness on the

component of velocity due to dip.

(2) Study the effects of non-unit viscosity ratios on the bubble configuration.

(3) integrate gravitational segregation and dispersion into a single computer program to determine both the configuration of the injected bubble and the recovery efficiency in a dipping system.

NOMENCLATURE

A = cross-sectional area (cm^2)

$B = 9.88 \times 10^{-7} \frac{K \cdot \Delta\rho \cdot g \cdot \sin\theta}{\overline{\mu} \cdot \phi}$

C = concentration (volume fraction)

D = coefficient of molecular diffusion of fluids in porous medium (cm^2/sec)

$\text{erfc}(\xi)$ = complementary error function of ξ

$$\text{erfc}(\xi) = \frac{2}{\sqrt{\pi}} \int_{\xi}^{\infty} e^{-w^2}\, dw$$

g = gravitational acceleration (cm/sec^2)

h = aquifer thickness (cm)

K = permeability (darcies)

L = total length (cm)

n = exponent

p = pressure (atm)

q = volumetric flow rate (cc/sec)

$Q = q/(2 \cdot \pi \cdot h \cdot \phi)$ (cm^2/sec)

r = radius (cm)

S = density gradient (gm/cm^4)

t = time (sec)

V = velocity (cm/sec)

$\overline{V}$ = average velocity (cm/sec)

$\left[\frac{q_i \cdot t}{A \cdot L \cdot \phi}\right]$ = Dimensionless pore volumes injected

$\overline{2XL}$ = Projection of the interface on the horizontal (cm)

Greek

μ = viscosity (cp)

$\bar{\mu}$ = average viscosity of the injected and native fluids (poise)

ρ = density (gm/cc)

$\Delta\rho$ = density difference between native and injected fluids (gm/cc)

α = longitudinal dispersivity coefficient (cm)

θ = dip angle (degrees)

ϕ = porosity (fraction)

Φ = potential (atm)

$$\psi = \left[\frac{K \cdot g \cdot \Delta\rho \cdot t}{\bar{\mu} \cdot \phi \cdot h}\right] \left[\frac{(\bar{\mu})^{2/3} \cdot S}{(\Delta\rho)^{5/3} \cdot (g)^{1/3}}\right]^{0.5}$$

Subscripts

d = downdip

g = gravity

i = injection

o = initial

u = updip

x = direction coinciding with dip

y = direction perpendicular to dip

SELECTED REFERENCES

1. Kimbler, O. K.; Kazmann, R. G.; and Whitehead, W. R.: "Saline Aquifers--Future Storage Reservoirs for Fresh Water?". Presented at the Second International Symposium on Underground Waste Management and Artificial Recharge, New Orleans, Louisiana; September, 1973.

2. Kohout, F. A.: "Reorientation of Our Saline Water Resources Thinking," Water Resources Research, Vol. 6, No. 5; October, 1970.

3. Cederstrom, D. J.: "Artificial Recharge of a Brackish Water Well," The Commonwealth; December, 1947.

4. Moulder, E. A., and Frazor, D. R.: "Artificial-Recharge Experiments at McDonald Well Field, Amarillo, Texas," Texas Board of Water Engineers, Bulletin 5701; January, 1957.

5. Esmail, O. J.: "Investigation of the Technical Feasibility of Storing Fresh Water in Saline Aquifers," M.S. Thesis, Louisiana State University, Baton Rouge; August, 1966.

6. Green, D. W., and Cox, R. L.: "Storage of Fresh Water in Underground Reservoirs Containing Saline Water--Phase II," Kansas Water Resources Research Institute, Contribution No. 36; December, 1968.

7. Esmail, O. J., and Kimbler, O. K.: "Investigation of the Technical Feasibility of Storing Fresh Water in Saline Aquifers," Journal of Water Resources Research, 1967, Vol. 3, No. 3, pp. 683-695.

8. Kumar, A., and Kimbler, O. K.: "Dispersion and Gravity Segregation of Miscible Fluids in Porous Media for Stratified Radial Flow Systems," Journal of Water Resources Research, 1970, Vol. 6, No. 6, pp. 1689-1700.

9. Francis, J. L., Jr.: "An Investigation of the Factors Influencing the Storage of Fresh Water in Inclined Saline Aquifers," M.S. Thesis, Louisiana State University, Baton Rouge; January, 1970.

10. Painter, T. R.: "Unequal Density Miscible Displacements in Thin Homogeneous Tilted Beds," M.S. Thesis, Louisiana State University, Baton Rouge; December, 1971.

11. Gelhar, L. W.; Wilson, J. L.; Miller, J. S.; and Hamrick, J. M.: "Density Induced Mixing in Confined Aquifers," EPA Water Pollution Control Research Series 16060 ELJ 03/72; March, 1972.

12. Esmail, W. J.: "The Effect of Flux and Gravitational Forces on Miscible Displacement in a Thin Homogeneous Bed," M.S. Thesis, Louisiana State University, Baton Rouge; August, 1973.

13. Whitehead, W. R.: "Storage of Fresh Water in Saline Aquifers Using a Well Field," Ph.D. Dissertation, Louisiana State University, Baton Rouge; August, 1974.

14. Langhetee, E. J.: "The Use of Bounding Wells to Control Flux in Underground Water Storage Projects," M.S. Thesis, Louisiana State University, Baton Rouge; August, 1974.

15. de Josselin de Jong, G.: "Longitudinal and Transverse Diffusion in Granular Deposits," Transactions, AGU, Vol. 39, No. 1, February, 1958, pp. 67-74.

16. Pozzi, A. L., and Blackwell, R. J.: "Design of Laboratory Models for Study of Miscible Displacement," Transactions, SPE of AIME, Vol. 228, Pt. II, March, 1963, pp. 28-40.

17. Raimondi, P.; Gardner, G. H. F.; and Petrick, C. B.: "Effect of Pore Structure and Molecular Diffusion on the Mixing of Miscible Liquids Flowing in Porous Media," Preprint 43, AIChE-SPE Joint Symposium on Fundamental Concepts of Miscible Fluid Displacement: Part II, 52nd Annual Meeting, San Francisco, Dec. 6-9, 1959.

18. Hoopes, J. A., and Harleman, D. R. F.: "Dispersion in Radial Flow From a Recharge Well," Journal of Geophysical Research, Vol. 72, No. 14, July, 1967, pp. 3595-3607.

19. Bentsen, R. G., and Nielsen, R. F.: "A Study of Plane Radial Miscible Displacement in a Consolidated Porous Medium," Transactions, SPE of AIME, Vol. 222, Pt. II, March, 1965, pp. 1-5.

20. Brigham, W. E.; Reed, P. W.; and Dew, J. N.: "Experiments on Mixing during Miscible Displacement in Porous Media," Transactions, SPE of AIME, Vol. 222, Pt. II, March, 1961, pp. 1-8.

21. Gardner, G. H. F.; Downie, J.; and Wyllie, M. R. M.: "Problems in the Recovery of Gas from Aquifers Used for Gas Storage," Journal of Institute of Petroleum, Vol. 48, No. 457, January, 1962, pp. 1-6.

APPENDIX A

DATA FROM THE FRONTAL MIGRATION OF THE LOWER SURFACE OF THE INJECTED BUBBLE

TABLE A-1

Run No. 1-1: Data from the Lower Surface of the Bubble

Bubble Size = 598.47 cc Density Difference = 0.0695 gm/cc

Dimensionless P.V.'s injected = 1.929×10^{-2}

Dip Angle = 10°

$B = 3.096 \times 10^{-4}$ cm/sec where $B \equiv 9.88 \times 10^{-7} \frac{K \cdot \Delta\rho \cdot g \cdot \sin\theta}{\bar{\mu} \cdot \phi}$

Inc.	Position of Bubble Center (cm)	ΔX (cm)	Time (sec)	ΔT (sec)	Velocity (cm/sec)
1	1.425	-	-	-	-
2	2.300	0.875	4,550	4,550	1.923×10^{-4}
3	3.400	1.100	9,920	5,370	2.048×10^{-4}
4	5.500	2.100	19,920	10,000	2.10×10^{-4}
5	6.375	0.875	23,946	4,026	2.173×10^{-4}

Average velocity, $\bar{V}_g = 2.06 \times 10^{-4}$ cm/sec

$\frac{\bar{V}_g}{B} = 0.6658$

TABLE A-2

Run No. 1-3: Data from the Lower Surface of the Bubble

Bubble Size = 598.47 cc Density Difference = 0.0695 gm/cc

Dimensionless P.V.'s injected = 1.929×10^{-2}

Dip Angle = 20°

$B = 6.098 \times 10^{-4}$ cm/sec where $B \equiv 9.88 \times 10^{-7} \frac{K \cdot \Delta\rho \cdot g \cdot \sin\theta}{\bar{\mu} \cdot \phi}$

Inc.	Position of Bubble Center (cm)	ΔX (cm)	Time (sec)	ΔT (sec)	Velocity (cm/sec)
1	1.525	-	-	-	-
2	2.350	0.825	3,016	3,016	2.735×10^{-4}
3	4.475	2.125	7,471	4,455	4.770×10^{-4}
4	6.500	2.025	12,541	5,070	3.994×10^{-4}
5	7.625	1.125	17,041	4,500	2.500×10^{-4}
6	9.800	2.175	22,881	5,840	3.724×10^{-4}

Average velocity, $\bar{V}_g = 3.545 \times 10^{-4}$ cm/sec

$\frac{\bar{V}_g}{B} = 0.5780$

TABLE A-3

Run No. 3-2: Data from the Lower Surface of the Bubble

Bubble Size = 598.47 cc Density Difference = 0.0687 gm/cc

Dimensionless P.V.'s injected = 1.929×10^{-2}

Dip Angle = 15°

$B = 4.1647 \times 10^{-4}$ cm/sec where $B \equiv 9.88 \times 10^{-7} \frac{K \cdot \Delta\rho \cdot g \cdot \sin\theta}{\bar{\mu} \cdot \phi}$

Inc.	Position of Bubble Center (cm)	ΔX (cm)	Time (sec)	ΔT (sec)	Velocity (cm/sec)
1	2.200	-	-92	-	-
2	2.900	0.700	4,223	4,315	1.622×10^{-4}
3	4.325	1.425	8,758	4,535	3.142×10^{-4}
4	6.800	2.475	17,778	9,020	2.744×10^{-4}
5	8.625	1.825	26,268	8,490	2.150×10^{-4}
6	10.500	1.875	34,703	8,435	2.223×10^{-4}

Average velocity, $\bar{V}_g = 2.376 \times 10^{-4}$ cm/sec

$\frac{\bar{V}_g}{B} = 0.5706$

TABLE A-4

Run No. 1-4: Data from the Lower Surface of the Bubble

Bubble Size = 1832.82 cc Density Difference = 0.0695 gm/cc

Dimensionless P.V.'s injected = 5.904×10^{-2}

Dip Angle = 10°

$B = 3.096 \times 10^{-4}$ cm/sec where $B \equiv 9.88 \times 10^{-7} \frac{K \cdot \Delta\rho \cdot g \cdot \sin\theta}{\bar{\mu} \cdot \phi}$

Inc.	Position of Bubble Center (cm)	ΔX (cm)	Time (sec)	ΔT (sec)	Velocity (cm/sec)
1	2.025	-	-	-	-
2	2.300	0.275	4,582	4,582	0.6×10^{-4}
3	3.750	1.450	10,232	5,650	2.566×10^{-4}
4	5.550	1.800	17,892	7,660	2.349×10^{-4}
5	6.625	1.075	22,462	4,570	2.352×10^{-4}
6	7.800	1.175	29,782	7,320	1.605×10^{-4}

Average velocity, $\bar{V}_g = 2.218 \times 10^{-4}$ cm/sec (excluding second increment)

$$\frac{\bar{V}_g}{B} = 0.7160$$

TABLE A-5

Run No. 1-5: Data from the Lower Surface of the Bubble

Bubble Size = 1832.82 cc Density Difference = 0.0695 gm/cc

Dimensionless P.V.'s injected = 5.904×10^{-2}

Dip Angle = 20°

$B = 6.098 \times 10^{-4}$ cm/sec where $B \equiv 9.88 \times 10^{-7} \frac{K \cdot \Delta\rho \cdot g \cdot \sin\theta}{\bar{\mu} \cdot \phi}$

Inc.	Position of Bubble Center (cm)	ΔX (cm)	Time (sec)	ΔT (sec)	Velocity (cm/sec)
1	2.125	-	-	-	-
2	3.400	1.275	3,641	3,641	3.502×10^{-4}
3	6.025	2.625	9,670	6,029	4.354×10^{-4}
4	8.450	2.425	15,130	5,460	4.441×10^{-4}
5	11.425	2.975	22,250	7,120	4.178×10^{-4}
6	13.000	1.575	26,190	3,940	3.997×10^{-4}
7	16.200	3.200	33,180	6,990	4.578×10^{-4}

Average velocity, $\bar{V}_g = 4.175 \times 10^{-4}$ cm/sec

$\frac{\bar{V}_g}{B} = 0.6810$

TABLE A-6

Run No. 3-1: Data from the Lower Surface of the Bubble

Bubble Size = 3029.77 cc Density Difference = 0.0687 gm/cc

Dimensionless P.V.'s injected = 9.765×10^{-2}

Dip Angle = 20°

$B = 5.5035 \times 10^{-4}$ cm/sec where $B \equiv 9.88 \times 10^{-7} \frac{K \cdot \Delta\rho \cdot g \cdot \sin\theta}{\bar{\mu} \cdot \phi}$

Inc.	Position of Bubble Center (cm)	ΔX (cm)	Time (sec)	ΔT (sec)	Velocity (cm/sec)
1	1.75	-	121	-	-
2	4.50	2.750	7,281	7,160	3.841×10^{-4}
3	7.225	2.725	13,386	6,105	4.464×10^{-4}
4	10.40	3.175	20,056	6,670	4.760×10^{-4}
5	12.60	2.200	27,561	7,505	2.931×10^{-4}

Average velocity, $\bar{V}_g = 3.999 \times 10^{-4}$ cm/sec

$\frac{\bar{V}_g}{B} = 0.7270$

TABLE A-7

Run No. 3-3: Data from the Lower Surface of the Bubble

Bubble Size = 3029.77 cc Density Difference = 0.0687 gm/cc

Dimensionless P.V.'s injected = 9.765×10^{-2}

Dip Angle = 15°

$B = 4.1647 \times 10^{-4}$ cm/sec where $B \equiv 9.88 \times 10^{-7} \frac{K \cdot \Delta\rho \cdot g \cdot \sin\theta}{\bar{\mu} \cdot \phi}$

Inc.	Position of Bubble Center (cm)	ΔX (cm)	Time (sec)	ΔT (sec)	(cm/sec)
1	1.725	-	-76	-	-
2	3.125	1.40	6,894	6,970	2.009×10^{-4}
3	9.265	6.14	17,069	10,175	6.034×10^{-4}
4	10.475	1.21	32,389	15,320	0.7898×10^{-4}

Average velocity, $\bar{V}_g = 2.944 \times 10^{-4}$ cm/sec

$\frac{\bar{V}_g}{B} = 0.7069$

TABLE A-8

Run No. 4-1, Data from the Lower Surface of the Bubble

Bubble Size = 2393.89 cc Density Difference = 0.074 gm/cc

Dimensionless P.V.'s injected = 7.72×10^{-2}

Dip Angle = 5°

$B = 1.5897 \times 10^{-4}$ cm/sec where $B \equiv 9.88 \times 10^{-7} \frac{K \cdot \Delta\rho \cdot g \cdot \sin\theta}{\bar{\mu} \cdot \phi}$

Inc.	Position of Bubble Center (cm)	ΔX (cm)	Time (sec)	ΔT (sec)	Velocity (cm/sec)
1	1.80	-	-60	-	
2	2.85	1.05	14,305	14,365	0.7309×10^{-4}
3	3.525	0.675	21,825	7,520	0.8976×10^{-4}
4	5.050	1.525	36,245	14,420	1.0576×10^{-4}

Average velocity, $\bar{V}_g = 0.8954 \times 10^{-4}$ cm/sec

$\frac{\bar{V}_g}{B} = 0.563$

TABLE A-9

Run No. 4-2, Data from the Lower Surface of the Bubble

Bubble Size = 598.47 cc Density Difference = 0.074 gm/cc

Dimensionless P.V.'s injected = 1.929×10^{-2}

Dip Angle = 5°

$B = 1.5897 \times 10^{-4}$ cm/sec where $B \equiv 9.88 \times 10^{-7} \frac{K \cdot \Delta\rho \cdot g \cdot \sin\theta}{\bar{\mu} \cdot \phi}$

Inc.	Position of Bubble Center (cm)	ΔX (cm)	Time (sec)	ΔT (sec)	Velocity (cm/sec)
1	1.650		-67		
2	1.925	0.275	8,773	8,840	0.3111×10^{-4}
3	2.900	0.975	17,948	9,175	1.063×10^{-4}
4	4.000	1.100	26,108	8,160	1.348×10^{-4}
5	4.800	0.800	34,643	8,535	0.9373×10^{-4}

Average velocity, $\bar{V}_g = 0.9148 \times 10^{-4}$ cm/sec

$\frac{\bar{V}_g}{B} = 0.5755$

APPENDIX B

DATA FROM THE FRONTAL MIGRATION OF THE UPPER SURFACE OF THE INJECTED BUBBLE

TABLE B-1

Run No. 1-1, Data from the Upper Surface of the Bubble

Bubble Size = 598.47 cc Density Difference = 0.0695 gm/cc

Dimensionless P.V.'s injected = 1.929×10^{-2}

Dip Angle = 10°

$B = 3.096 \times 10^{-4}$ cm/sec where $B \equiv 9.88 \times 10^{-7} \frac{K \cdot \Delta\rho \cdot g \cdot \sin\theta}{\bar{\mu} \cdot \phi}$

Inc.	Position of Bubble Center (cm)	ΔX (cm)	Time (sec)	ΔT (sec)	Velocity (cm/sec)
1	0.575	-	-		
2	0.325	-0.25	4,550	4,550	-0.549×10^{-4}
3	0.600	0.275	9,920	5,370	0.512×10^{-4}
4	0.800	0.20	19,920	10,000	0.200×10^{-4}
5	0.700	-0.10	23,946	4,026	-0.248×10^{-4}

Average velocity, $\bar{V}_g = -0.085 \times 10^{-4}$ cm/sec

$\frac{\bar{V}_g}{B} = -0.02745$

TABLE B-2

Run No. 1-3, Data from the Upper Surface of the Bubble

Bubble Size = 598.47 cc Density Difference = 0.0695 gm/cc

Dimensionless P.V.'s injected = 1.929×10^{-2}

Dip Angle = 20°

$B = 6.098 \times 10^{-4}$ cm/sec where $B \equiv 9.88 \times 10^{-7} \frac{K \cdot \Delta\rho \cdot g \cdot \sin\theta}{\bar{\mu} \cdot \phi}$

Inc.	Position of Bubble Center (cm)	ΔX (cm)	Time (sec)	ΔT (sec)	Velocity (cm/sec)
1	0.175				
2	0.300	0.125	3,016	3,016	1.4145×10^{-4}
3	0.825	0.525	7,471	4,455	1.178×10^{-4}
4	1.000	0.175	12,541	5,070	0.3452×10^{-4}
5	1.325	0.325	17,041	4,500	0.722×10^{-4}
6	1.225	-0.100	22,881	5,840	-0.171×10^{-4}

Average velocity, $\bar{V}_g = 0.4977 \times 10^{-4}$ cm/sec

$\frac{\bar{V}_g}{B} = 0.08162$

TABLE B-3

Run No. 3-2, Data from the Upper Surface of the Bubble

Bubble Size = 598.47 cc Density Difference = 0.0687 gm/cc

Dimensionless P.V.'s injected = 1.929×10^{-2}

Dip Angle = 15°

$B = 4.1647 \times 10^{-4}$ cm/sec where $B \equiv 9.88 \times 10^{-7} \frac{K \cdot \Delta\rho \cdot g \cdot \sin\theta}{\bar{\mu} \cdot \phi}$

Inc.	Position of Bubble Center (cm)	ΔX (cm)	Time (sec)	ΔT (sec)	Velocity (cm/sec)
1	0.575		-92		
2	-0.025	0.600	4,223	4,315	1.390×10^{-4}
3	0.425	0.450	8,758	4,535	0.992×10^{-4}
4	0.750	0.325	17,778	9,020	0.360×10^{-4}
5	0.700	-0.050	26,268	8,490	-0.0589×10^{-4}
6	0.675	-0.025	34,703	8,435	-0.0296×10^{-4}

Average velocity, $\bar{V}_g = 0.5309 \times 10^{-4}$ cm/sec

$\frac{\bar{V}_g}{B} = 0.1275$

TABLE B-4

Run No. 1-4, Data from the Upper Surface of the Bubble

Bubble Size = 1832.82 cc Density Difference = 0.0695 gm/cc

Dimensionless P.V.'s injected = 5.904×10^{-2}

Dip Angle = 10°

$B = 3.096 \times 10^{-4}$ cm/sec where $B \equiv 9.88 \times 10^{-7} \frac{K \cdot \Delta\rho \cdot g \cdot \sin\theta}{\bar{\mu} \cdot \phi}$

Inc.	Position of Bubble Center (cm)	ΔX (cm)	Time (sec)	ΔT (sec)	Velocity (cm/sec)
1	1.050				
2	0.865	-.175	4,582	4,582	-0.3819×10^{-4}
3	0.825	-.050	10,232	5,650	-0.0885×10^{-4}
4	0.875	0.050	17,892	7,660	0.0653×10^{-4}
5	0.950	0.075	22,462	4,570	0.1641×10^{-4}
6	1.100	0.150	29,782	7,320	0.2049×10^{-4}

Average velocity, $\bar{V}_g = -.00722 \times 10^{-4}$ cm/sec

$\frac{\bar{V}_g}{B} = -.00233$

TABLE B-5

Run No. 1-5, Data from the Upper Surface of the Bubble

Bubble Size = 1832.82 cc Density Difference = 0.0695 gm/cc

Dimensionless P.V.'s injected = 5.904×10^{-2}

Dip Angle = 20°

$B = 6.098 \times 10^{-4}$ cm/sec where $B \equiv 9.88 \times 10^{-7} \frac{K \cdot \Delta\rho \cdot g \cdot \sin\theta}{\bar{\mu} \cdot \phi}$

Inc.	Position of Bubble Center (cm)	ΔX (cm)	Time (sec)	ΔT (sec)	Velocity (cm/sec)
1	0.5				
2	0.85	0.35	3,641	3,641	0.9613×10^{-4}
3	0.80	-0.05	9,670	6,029	-0.08293×10^{-4}
4	0.975	0.175	15,130	5,460	0.3205×10^{-4}
5	1.375	0.40	22,250	7,120	0.5618×10^{-4}
6	1.775	0.40	26,190	3,940	1.015×10^{-4}
7	2.550	0.775	33,180	6,990	1.109×10^{-4}

Average velocity, $\bar{V}_g = 0.647 \times 10^{-4}$ cm/sec

$\frac{\bar{V}_g}{B} = 0.1061$

TABLE B-6

Run No. 3-1, Data from the Upper Surface of the Bubble

Bubble Size = 3029.77 cc Density Difference = 0.0687 gm/cc

Dimensionless P.V.'s injected = 9.765×10^{-2}

Dip Angle = 20°

$B = 5.5035 \times 10^{-4}$ cm/sec where $B \equiv 9.88 \times 10^{-7} \frac{K \cdot \Delta\rho \cdot g \cdot \sin\theta}{\bar{\mu} \cdot \phi}$

Inc.	Position of Bubble Center (cm)	ΔX (cm)	Time (sec)	ΔT (sec)	Velocity (cm/sec)
1	0.8		121		
2	0.625	-0.175	7,281	7,160	-0.2444×10^{-4}
3	0.625	0.0	13,386	6,105	0
4	1.2	0.575	20,056	6,670	0.8621×10^{-4}
5	1.4	0.20	27,561	7,505	0.2665×10^{-4}

Average velocity, $\bar{V}_g = 0.221 \times 10^{-4}$ cm/sec

$\frac{\bar{V}_g}{B} = 0.0402$

TABLE B-7

Run No. 3-3, Data from the Upper Surface of the Bubble

Bubble Size = 3029.77 cc Density Difference = 0.0687 gm/cc

Dimensionless P.V.'s injected = 9.765×10^{-2}

Dip Angle = 15°

$B = 4.1647 \times 10^{-4}$ cm/sec where $B \equiv 9.88 \times 10^{-7} \frac{K \cdot \Delta\rho \cdot g \cdot \sin\theta}{\bar{\mu} \cdot \phi}$

Inc.	Position of Bubble Center (cm)	ΔX (cm)	Time (sec)	ΔT (sec)	Velocity (cm/sec)
1	1.4		-76		
2	1.1	-0.30	6,894	6,970	-0.4304×10^{-4}
3	0.95	-0.15	17,069	10,175	-0.1474×10^{-4}
4	0.975	0.025	32,389	15,320	0.0163×10^{-4}

Average velocity, $\bar{V}_g = -0.1872 \times 10^{-4}$ cm/sec

$\frac{\bar{V}_g}{B} = -0.04495$

APPENDIX C

TRACINGS OF THE FRONTAL MIGRATION OF THE LOWER SURFACE OF THE INJECTED BUBBLE

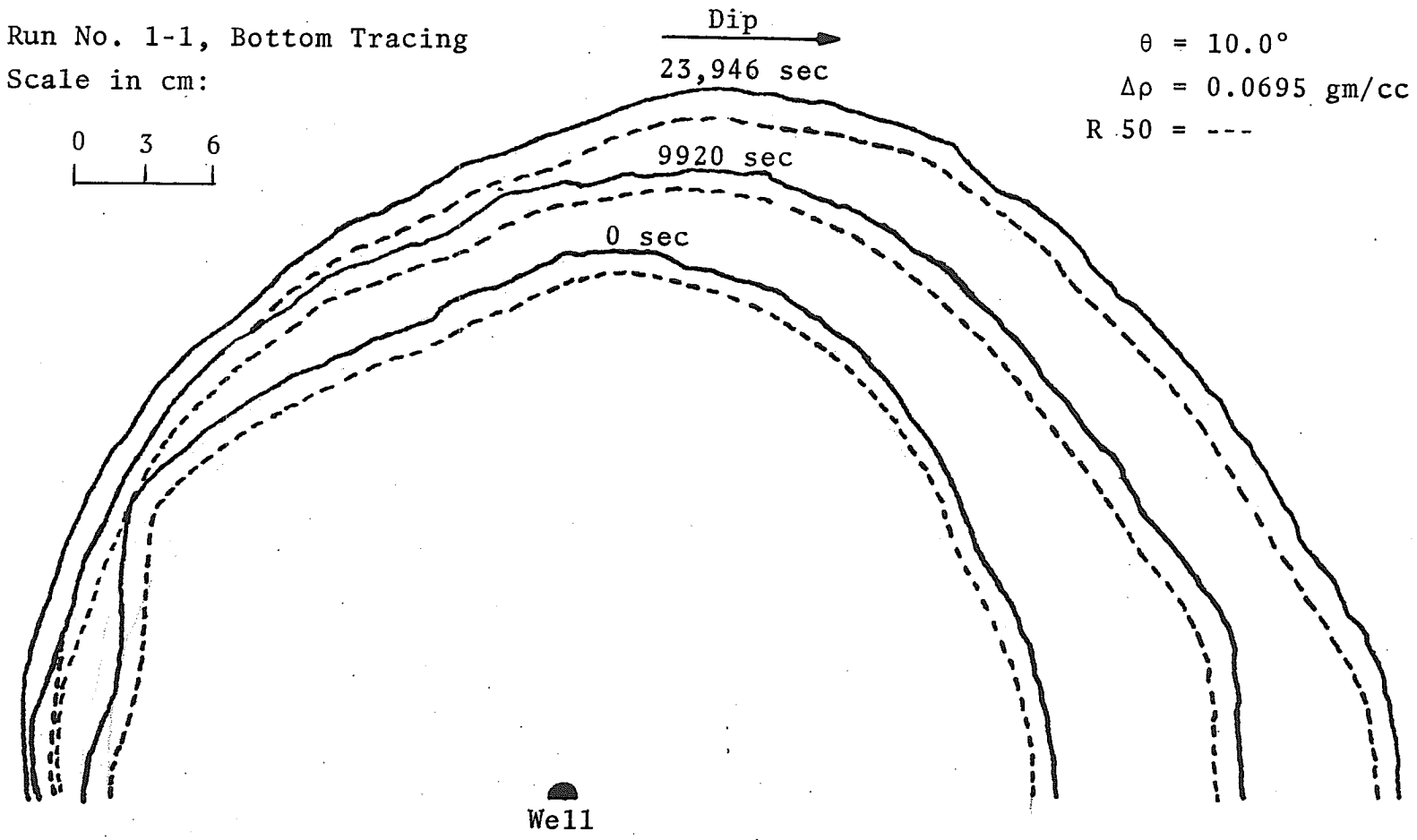
Run No. 1-1, Bottom Tracing
Scale in cm:
0 3 6
Dip
23,946 sec
9920 sec
0 sec
θ = 10.0°
Δρ = 0.0695 gm/cc
R 50 = ---
Well

Run No. 1-3, Bottom Tracing

Scale in cm

θ = 20.0°

Δρ = 0.0695 gm/cc

R 50 = ---

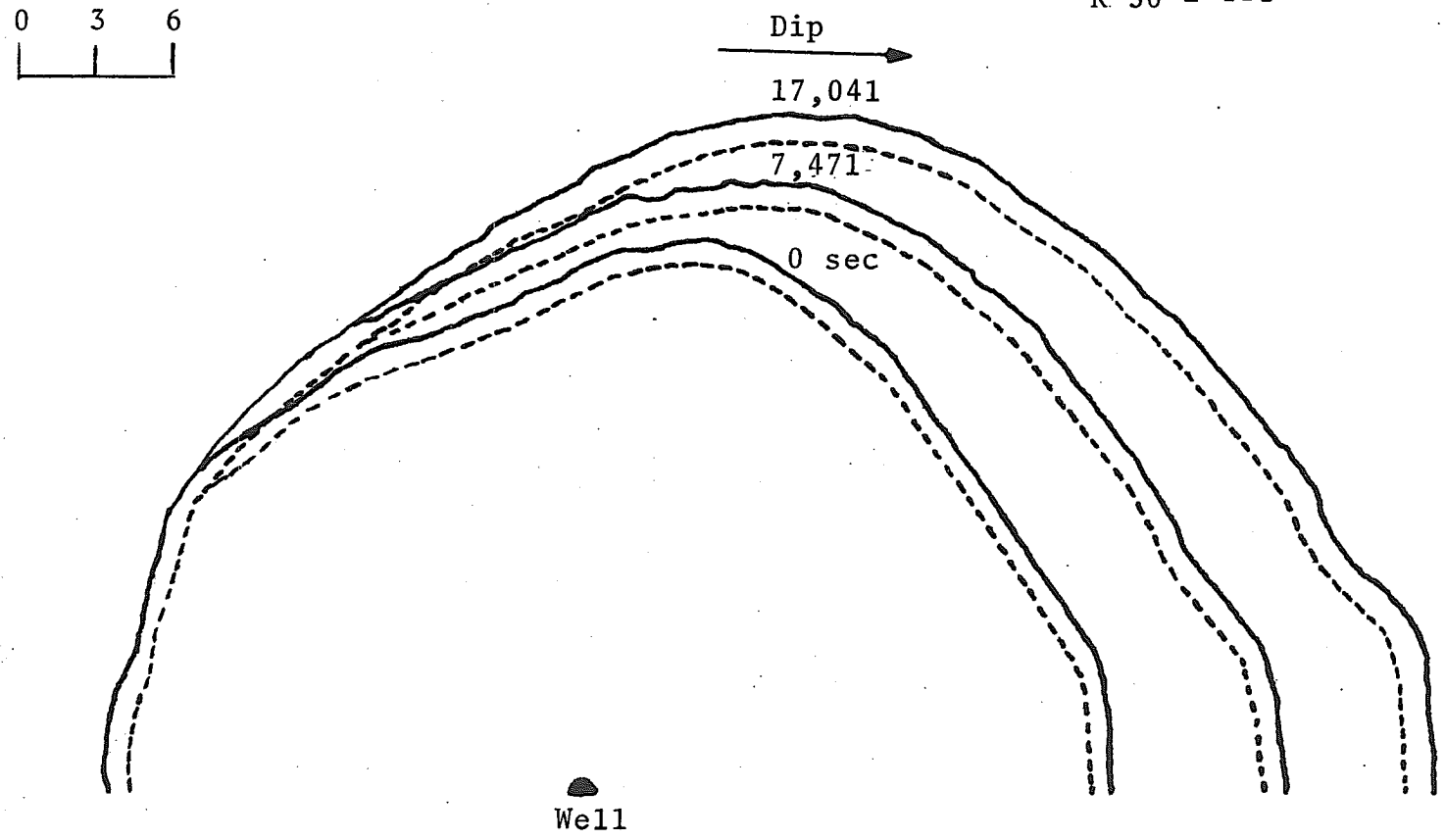

Run No. 1-4, Bottom Tracing

Scale in cm:

θ = 10.0°

Δρ = 0.0695 gm/cc

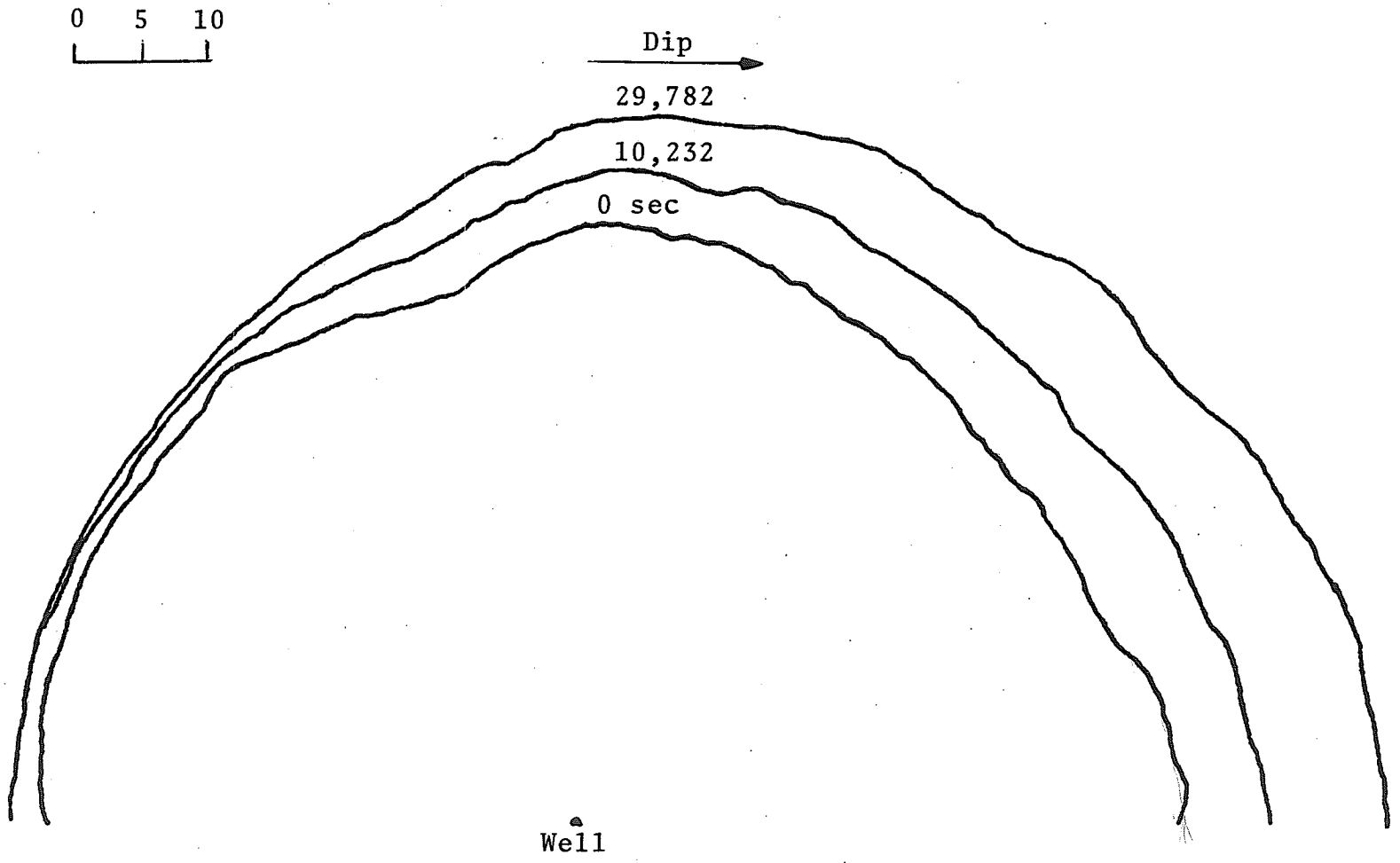

Run No. 1-5, Bottom Tracing

Scale in cm:

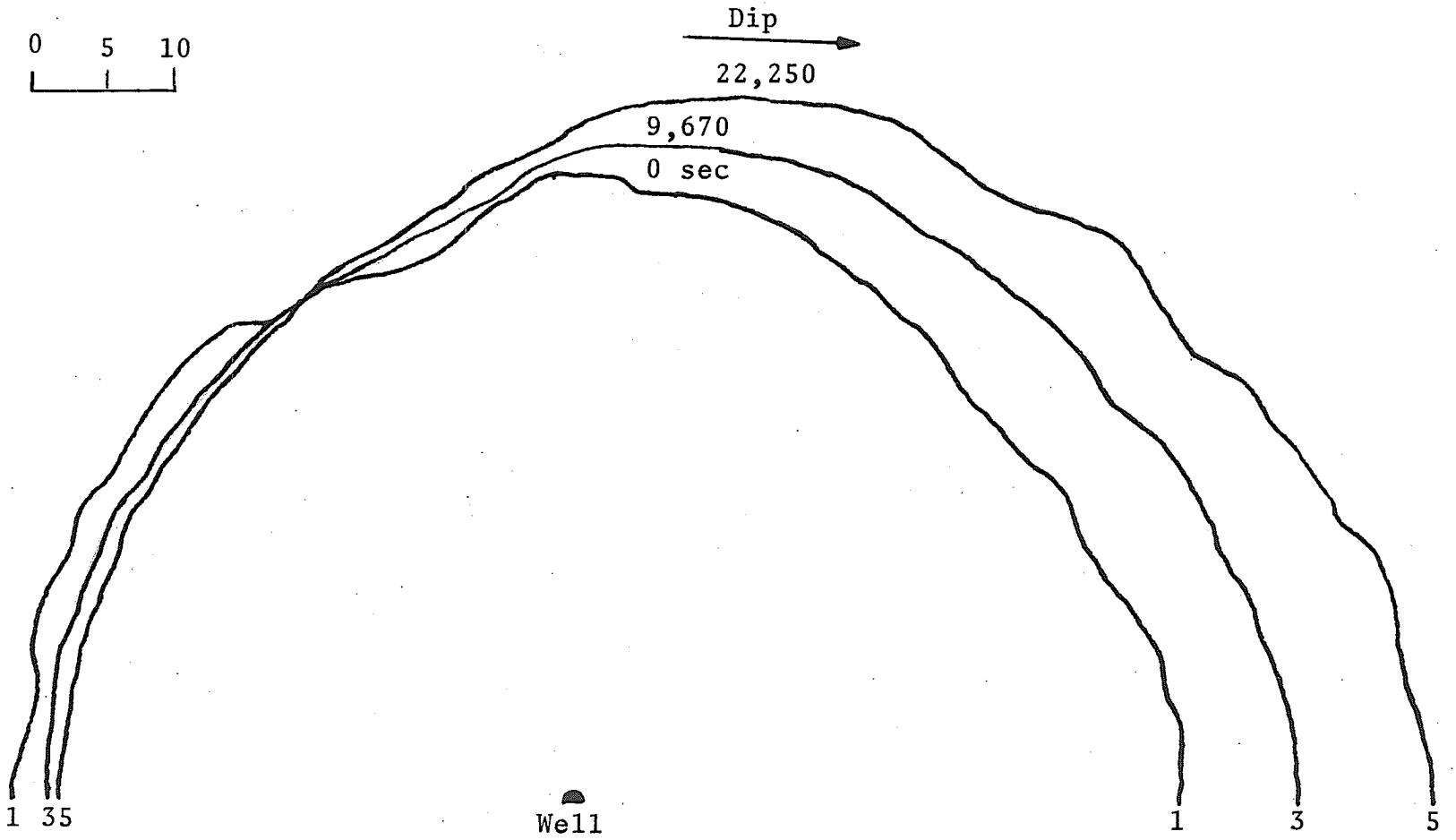

θ = 20.0°

$\Delta\rho$ = 0.0695 gm/cc

Run No. 3-1, Bottom Tracing

Scale in cm:

0 6 12

θ = 20.0°

$\Delta\rho$ = 0.0687 gm/cc

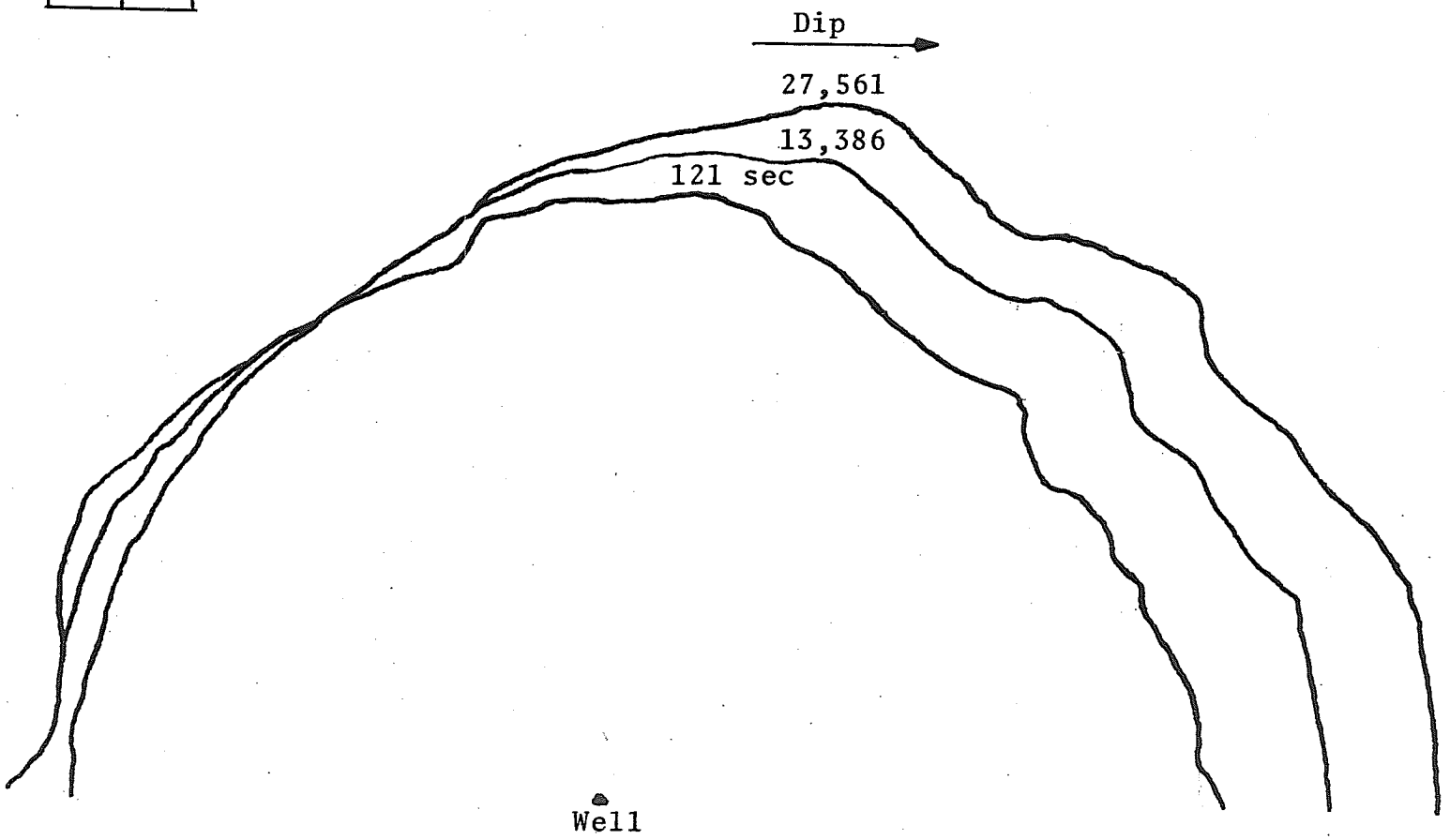

Run No. 3-2, Bottom Tracing

Scale in cm:

0 3 6

θ = 15.0°

Δρ = 0.0687 gm/cc

R 50 = ---

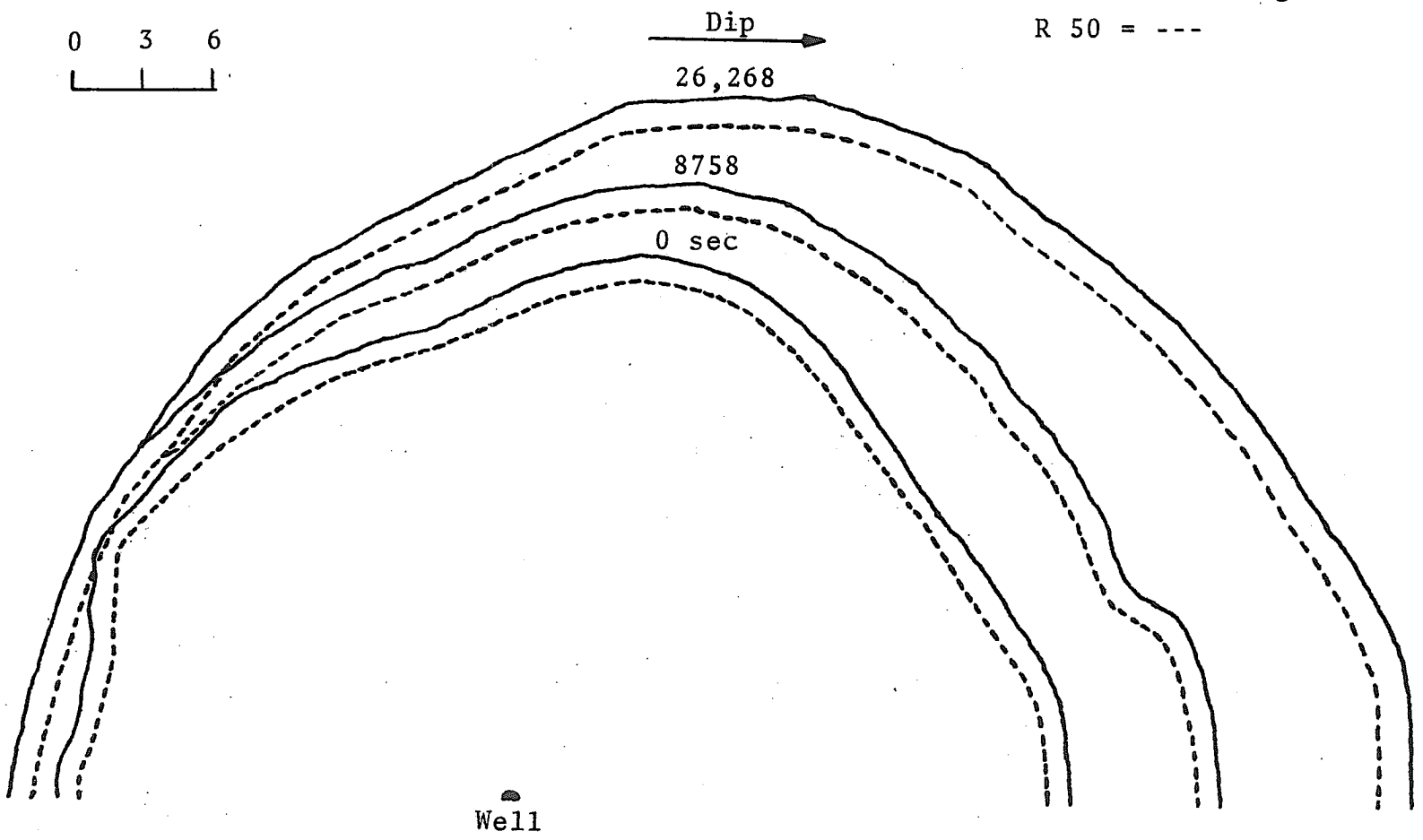

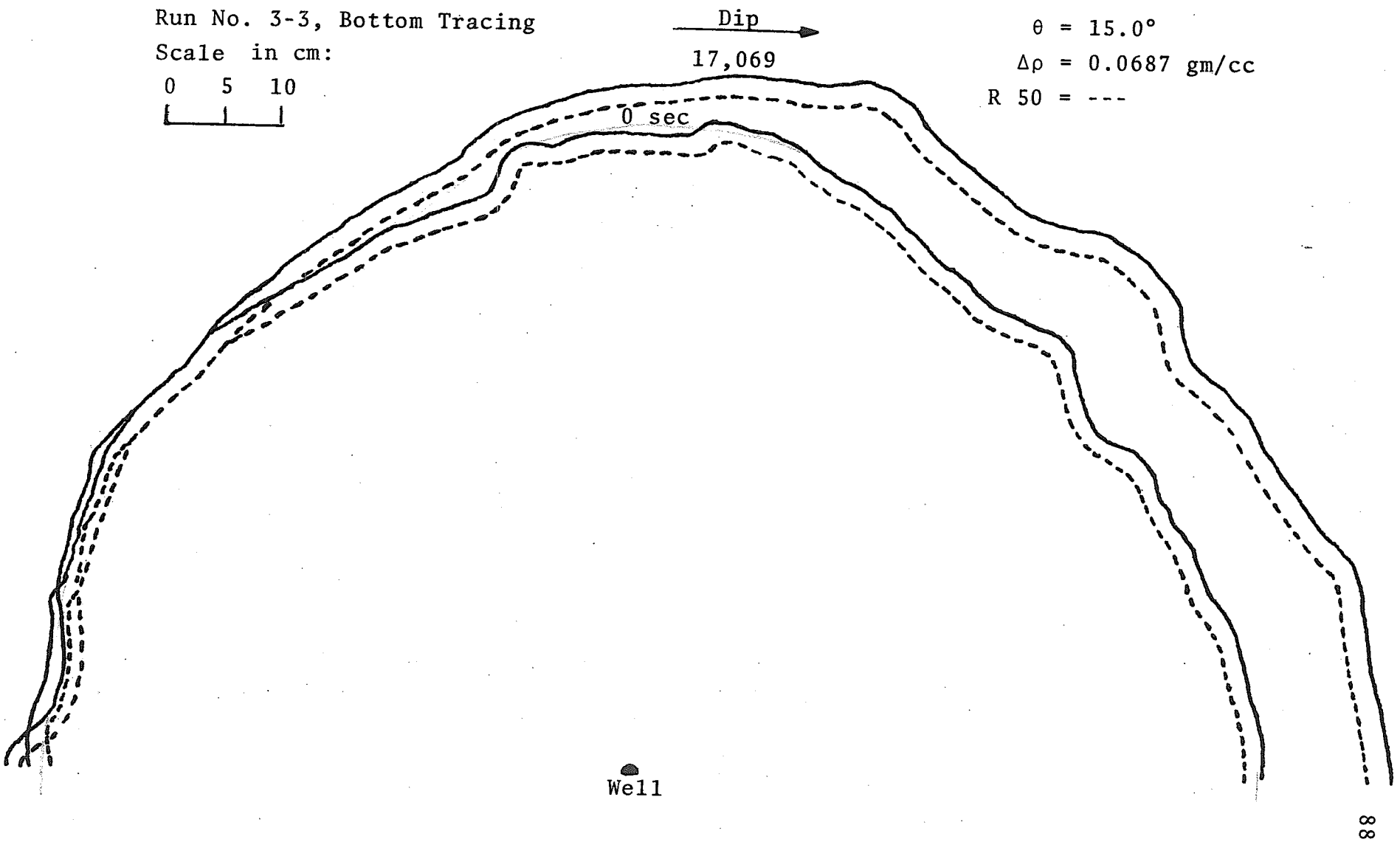
Run No. 3-3, Bottom Tracing
Scale in cm:
0 5 10
Dip
17,069
θ = 15.0°
Δρ = 0.0687 gm/cc
R 50 = ---
0 sec
Well

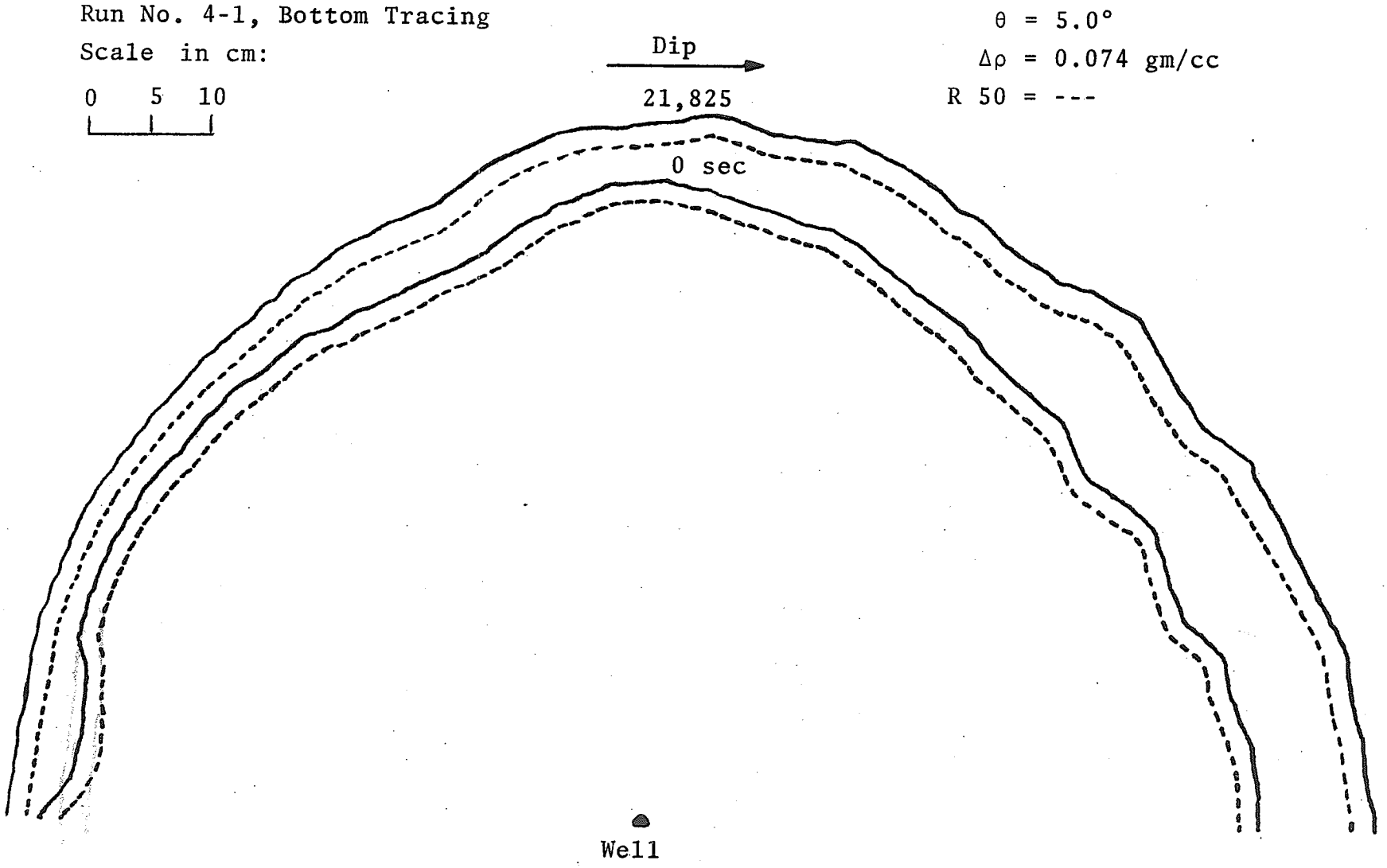
Run No. 4-1, Bottom Tracing
Scale in cm:
0 5 10
Dip
21,825
θ = 5.0°
Δρ = 0.074 gm/cc
R 50 = ---
0 sec
Well

Run No. 4-2, Bottom Tracing

Scale in cm:
0 3 6

θ = 5.0°
Δρ = 0.074 gm/cc
R 50 = ---

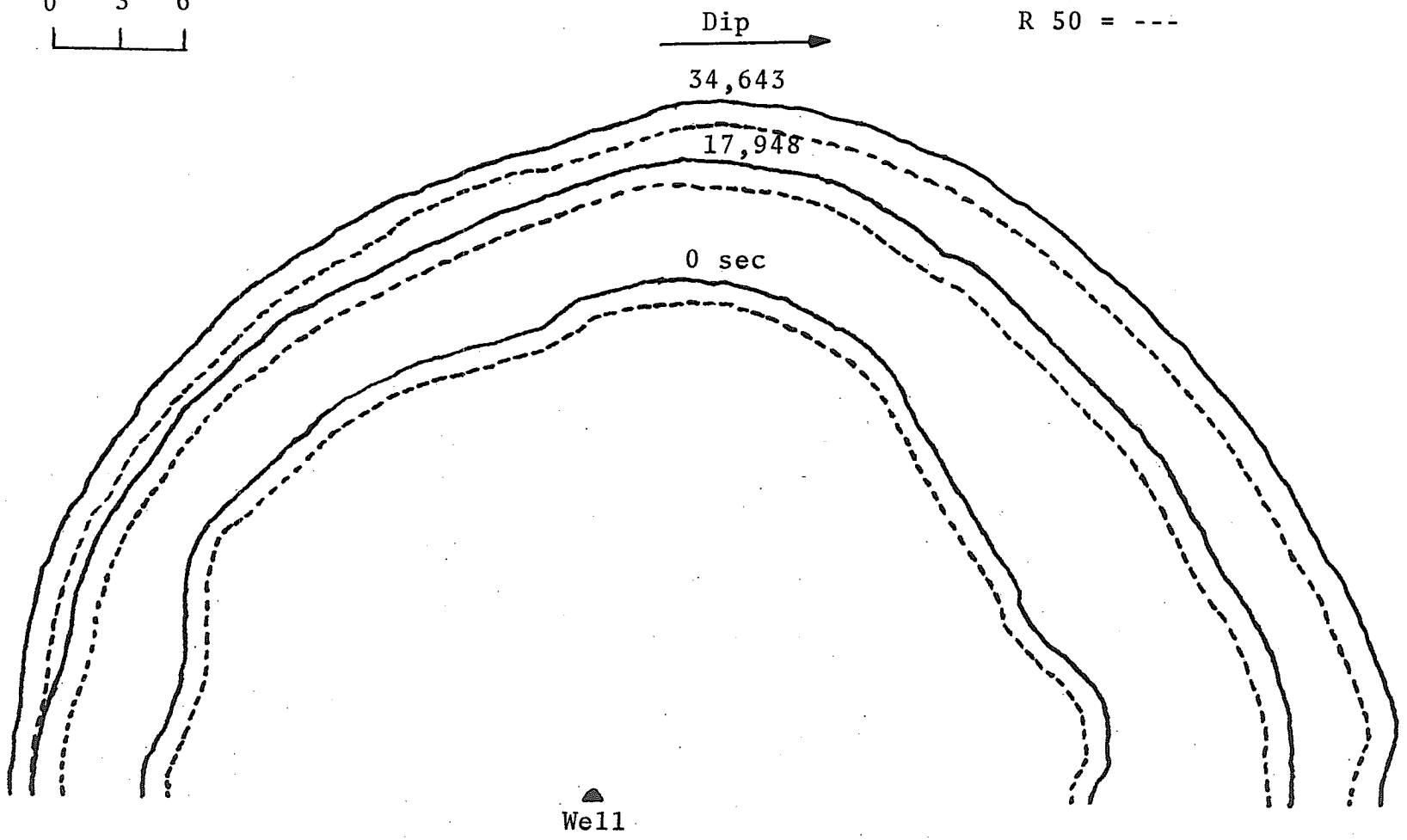

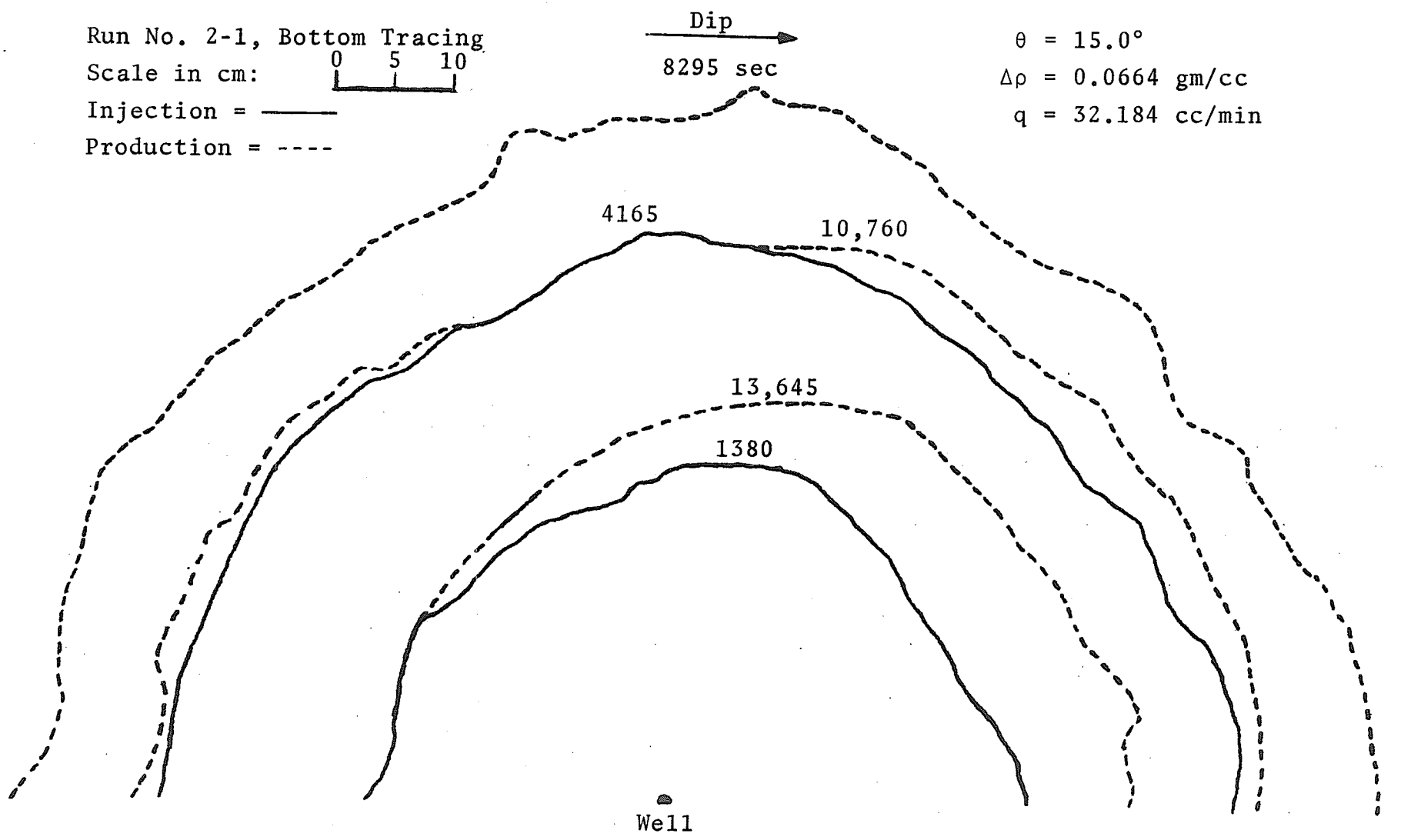
Run No. 2-1, Bottom Tracing
Scale in cm: 0 5 10
Injection = ———
Production = ----
Dip
8295 sec
θ = 15.0°
Δρ = 0.0664 gm/cc
q = 32.184 cc/min
4165
10,760
13,645
1380
Well

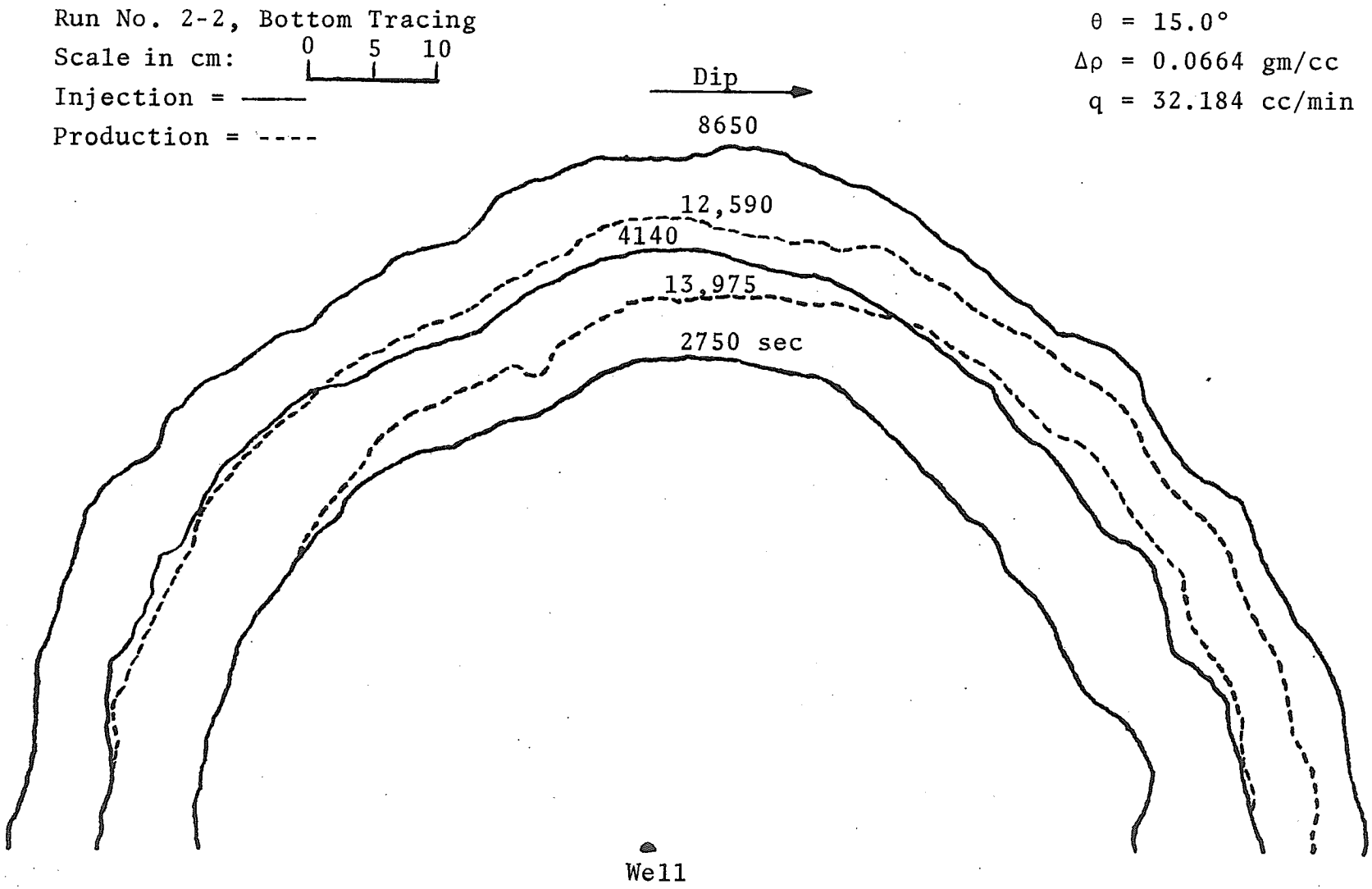
Run No. 2-2, Bottom Tracing
Scale in cm: 0 5 10
Injection = ——
Production = ----
θ = 15.0°
Δρ = 0.0664 gm/cc
q = 32.184 cc/min
Dip
8650
12,590
4140
13,975
2750 sec
Well

APPENDIX D

TRACINGS OF THE FRONTAL MIGRATION OF THE UPPER SURFACE OF THE INJECTED BUBBLE

Run No. 1-1, Top Tracing

Scale in cm:

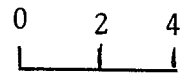

θ = 10.0°

Δρ = 0.0695 gm/cc

R 50 = ---

Run No. 1-3, Top Tracing

Scale in cm:

0 3 6

θ = 20.0°

Δρ = 0.0695 gm/cc

R 50 = ---

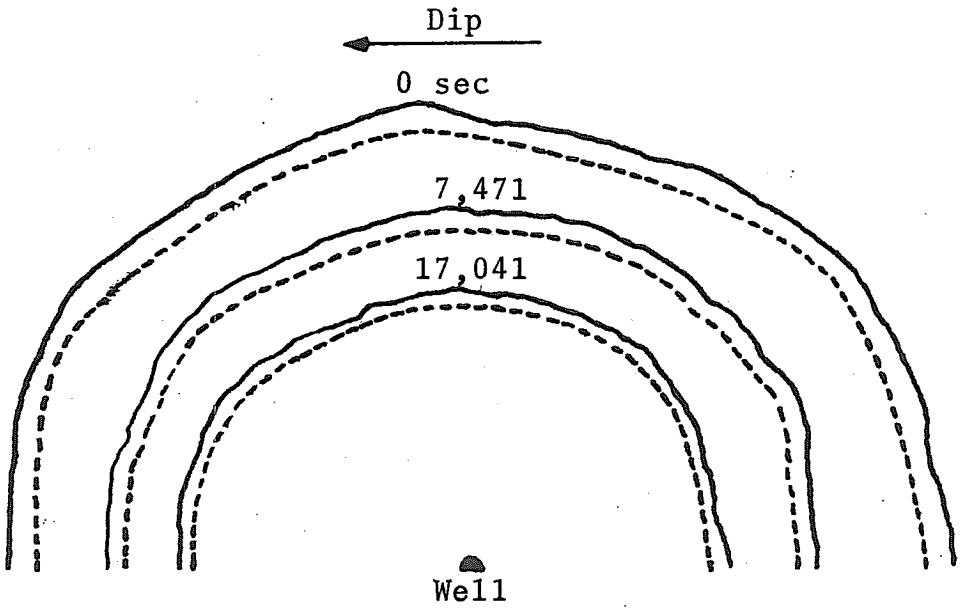

Run No. 1-4, Top Tracing

Scale in cm:

0 3 6

θ = 10.0°

Δρ = 0.0695 gm/cc

R 50 = ---

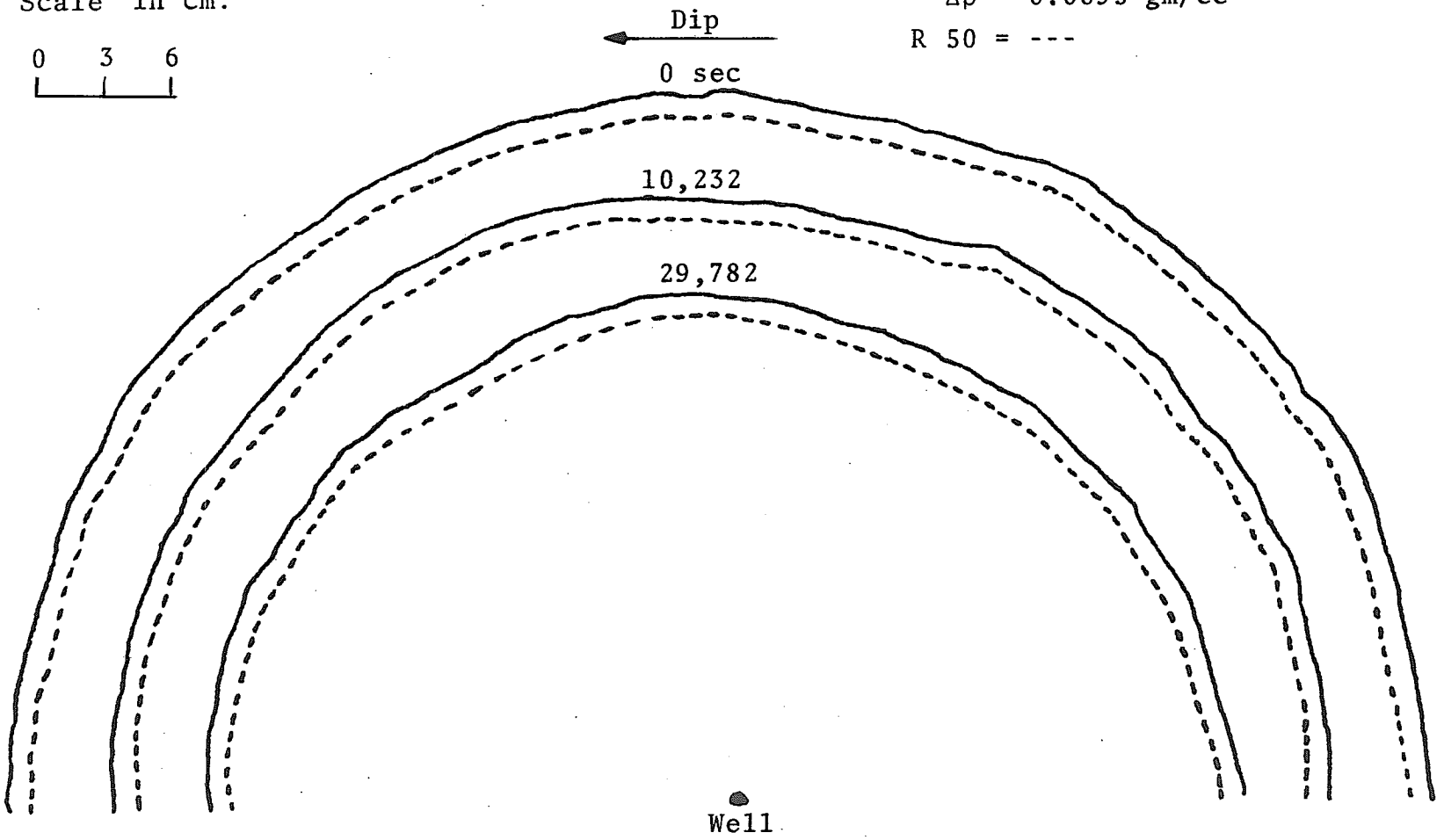

Run No. 1-5, Top Tracing

Scale in cm:

0 4 8

θ = 20.0°

Δρ = 0.0695 gm/cc

R 50 = ---

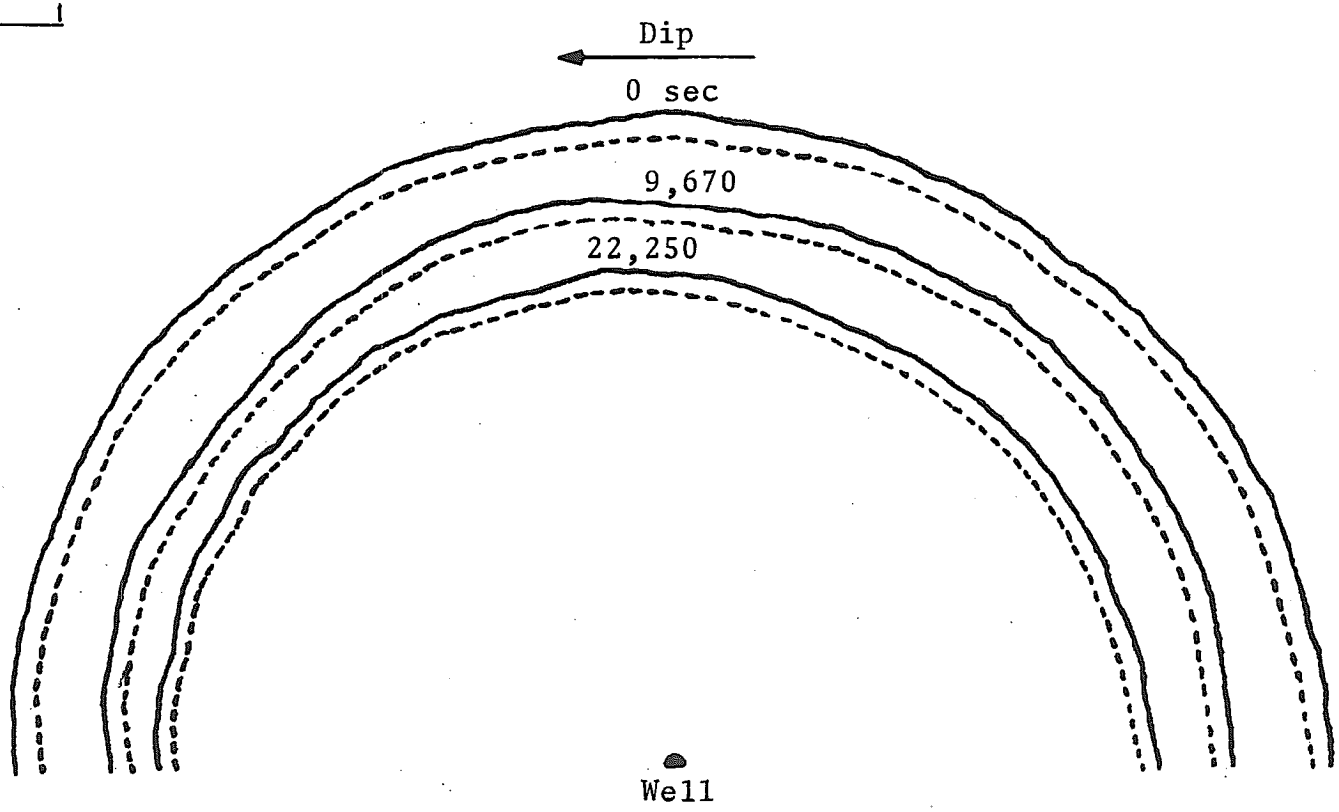

Run No. 3-1, Top Tracing

Scale in cm:

0 4 8

θ = 20.0°

Δρ = 0.0687 gm/cc

R 50 = ---

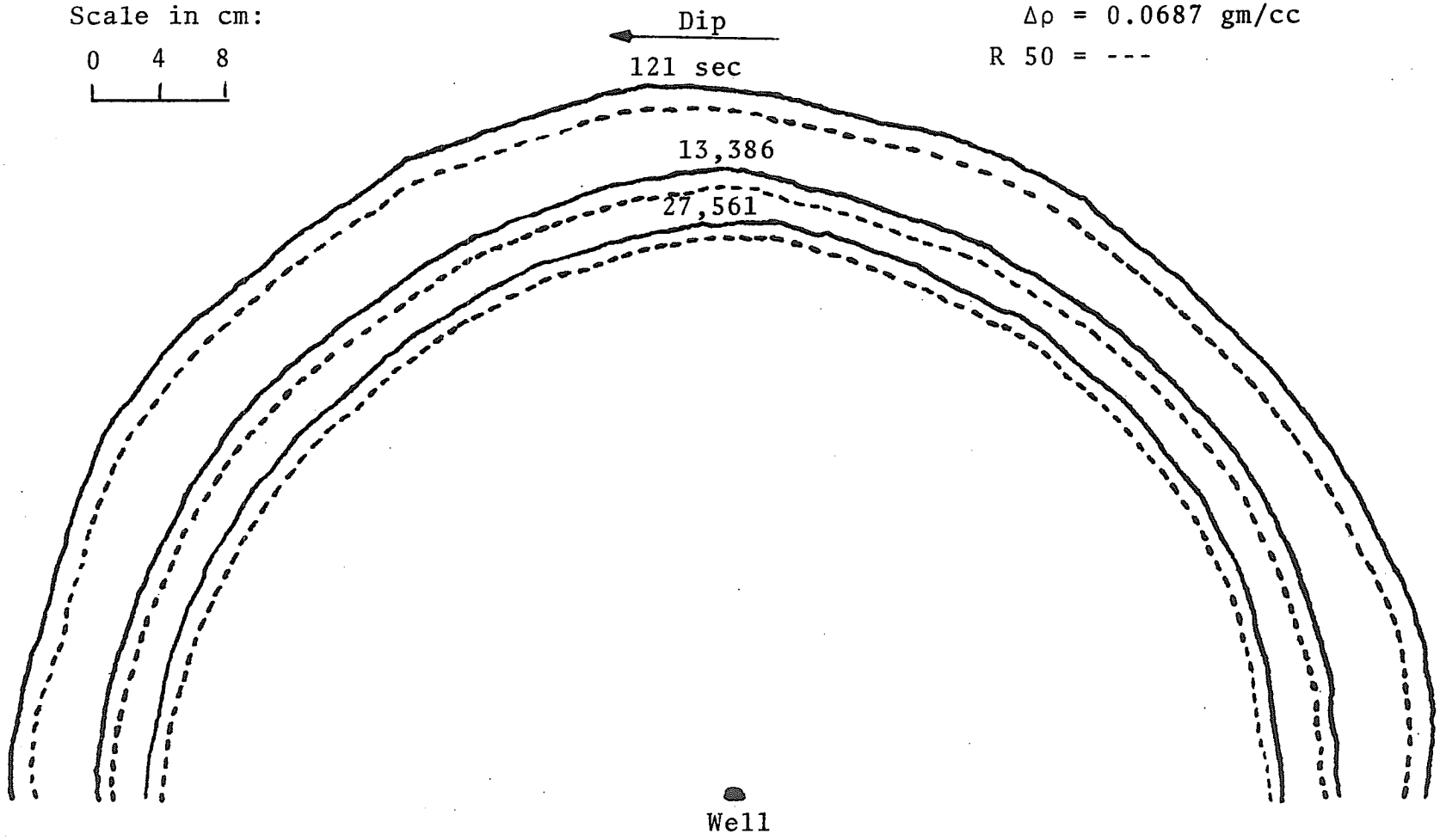

Run No. 3-2, Top Tracing

Scale in cm:

0 2 4

θ = 15.0°

Δρ = 0.0687 gm/cc

R 50 = ---

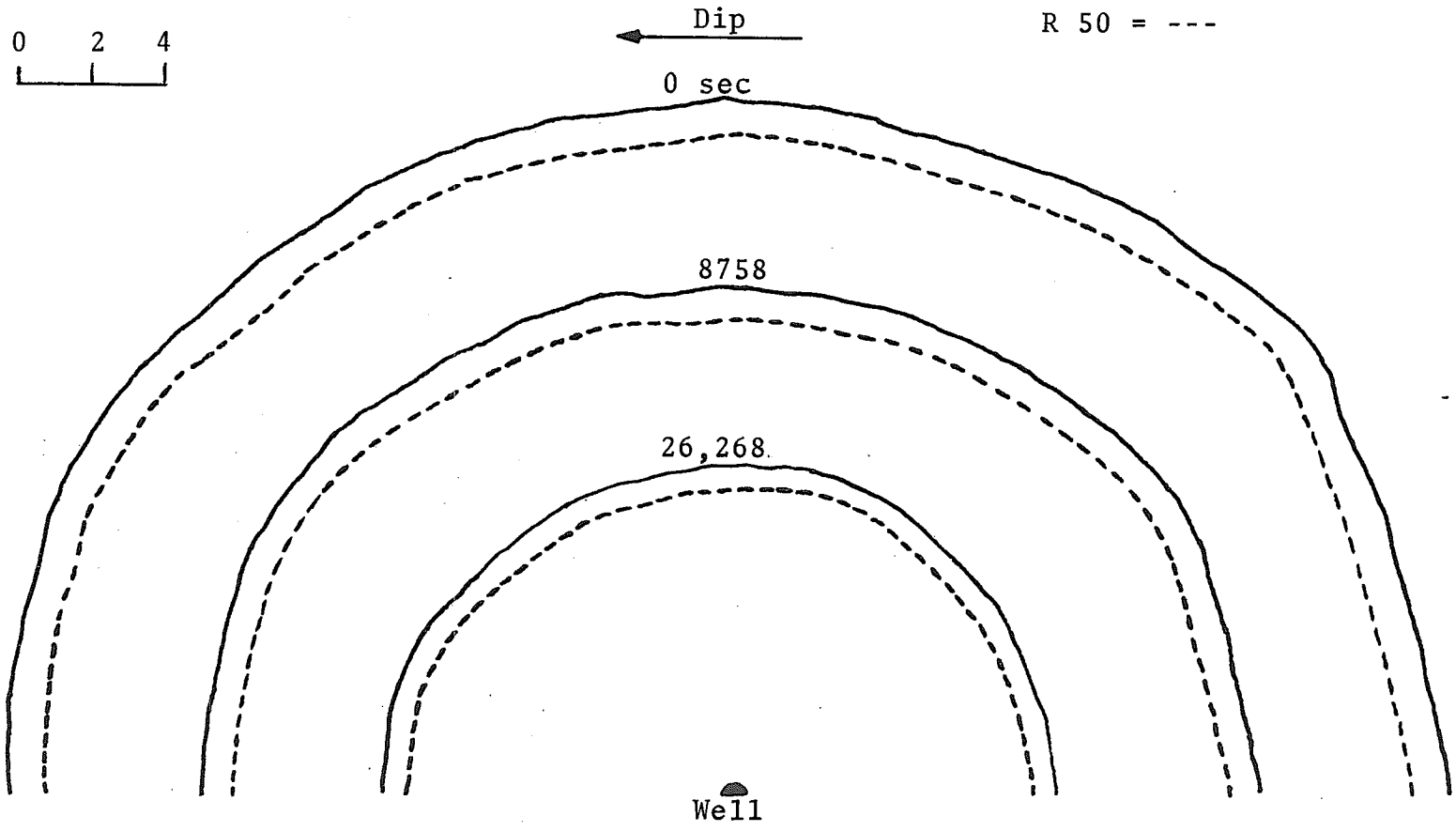

Run No. 3-3, Top Tracing

Scale in cm:

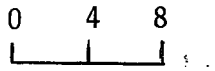

θ = 15.0°

Δρ = 0.0687 gm/cc

R 50 = ---

Run No. 2-1, Top Tracing
Scale in cm: 0 5 10
Injection = ——
Production = ----

θ = 15.0°
Δρ = 0.0664 gm/cc
q = 32.184 cc/min

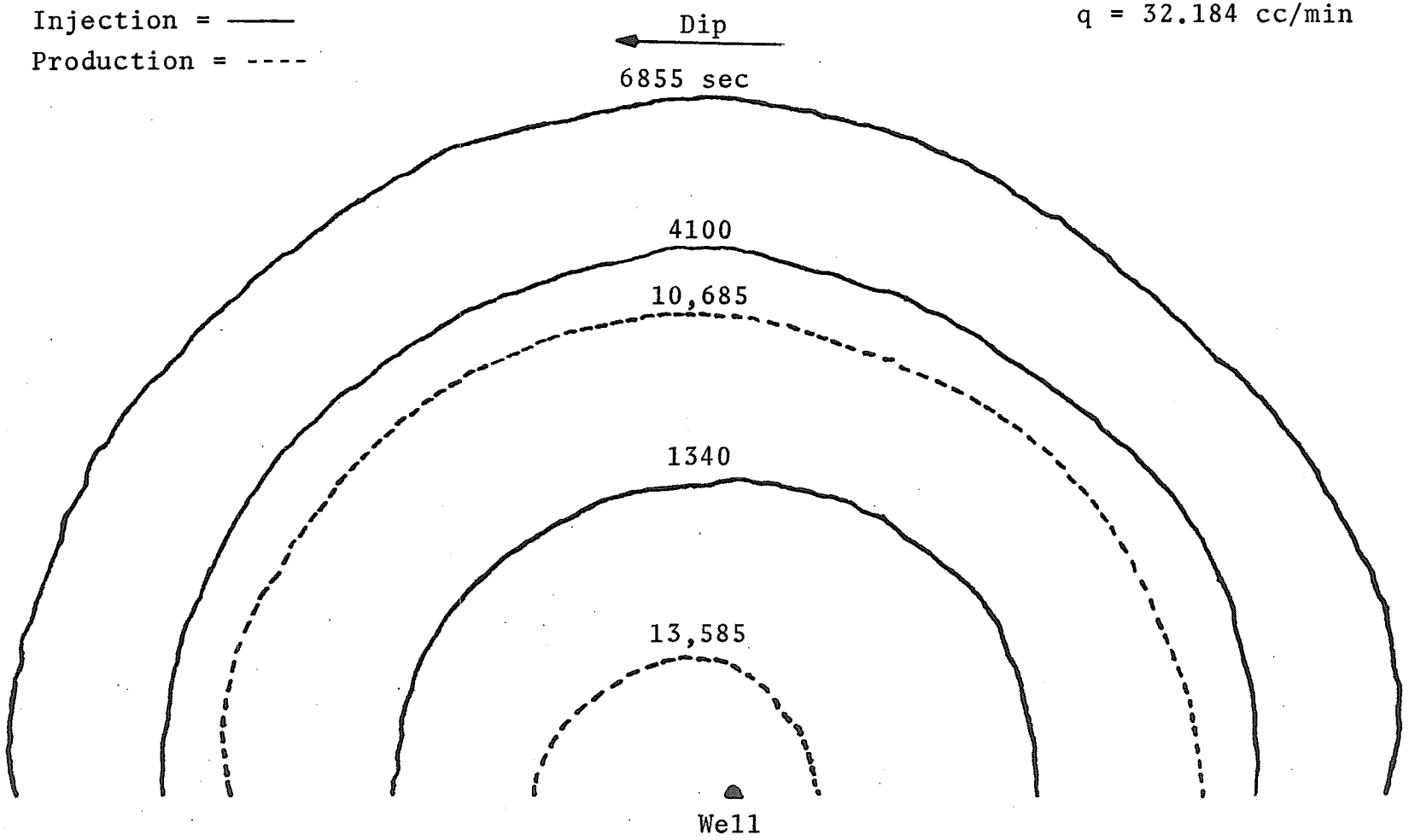

Run No. 2-2, Top Tracing

Scale in cm: 0 4 8

Injection = ——

Production = ----

θ = 15.0°

$\Delta\rho$ = 0.0664 gm/cc

q = 32.184 cc/min

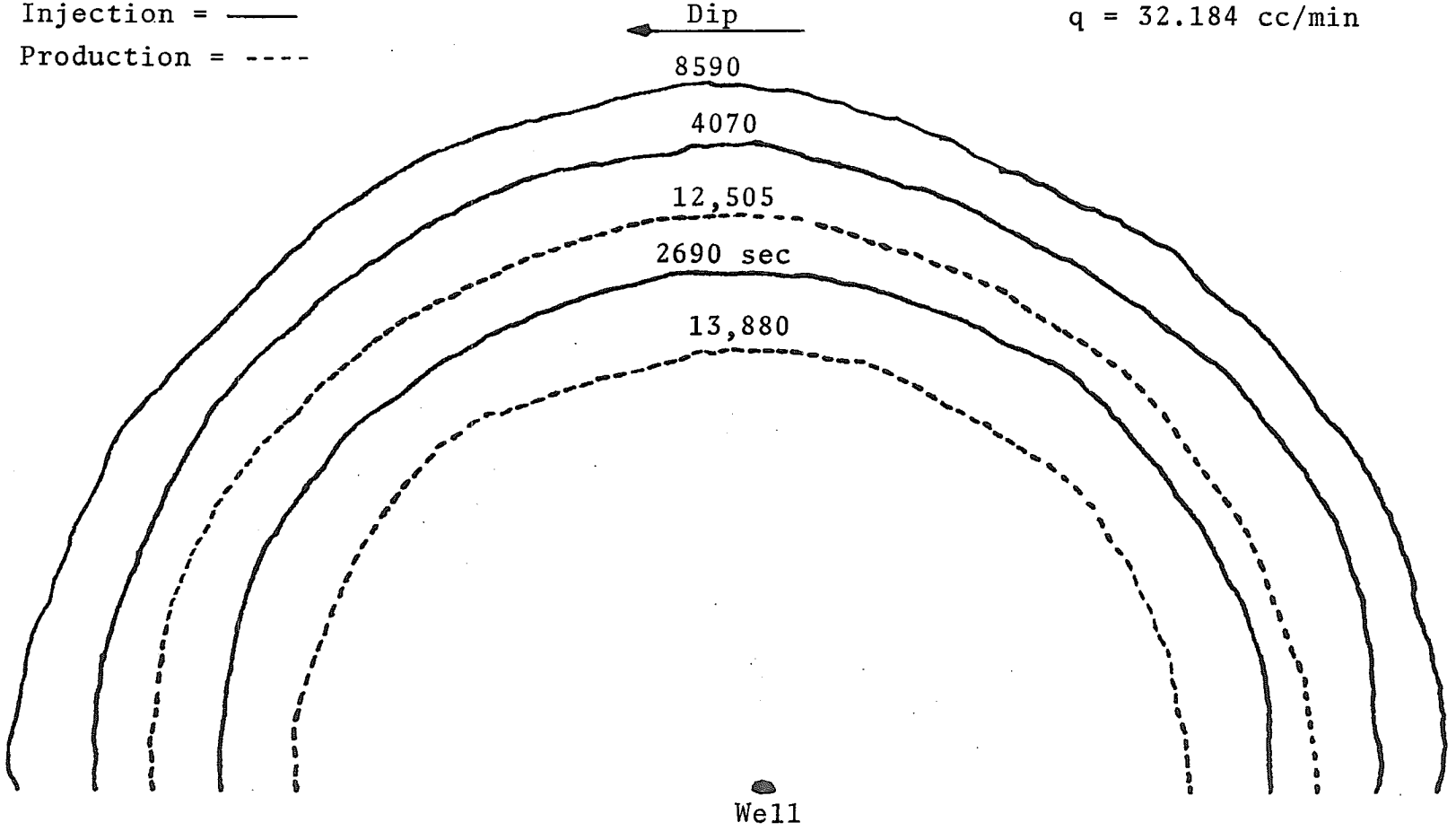

VITA

Joseph Anthony D'Amico, the son of Mr. and Mrs. Vincent C. D'Amico, was born May 1, 1948, in Plaquemine, Louisiana. He attended Shady Grove High School, graduating in May, 1966. Enrolled at Louisiana State University in Baton Rouge, he earned a Bachelor of Science degree in Petroleum Engineering in May, 1970.

He was then employed by Texaco, Inc., in New Orleans, Louisiana, as a production engineer. Deciding to further his education, he took a leave of absence from Texaco, Inc., in September, 1973. He returned to Louisiana State University in Baton Rouge, from which he will receive the Master of Science degree in Petroleum Engineering in August, 1975.

He is married to the former Catherine Cox of Falls Church, Virginia, a graduate of Loyola University in New Orleans, Louisiana.